

Can a Regional Climate Model Improve the Ability to Forecast the North American Monsoon?

CHRISTOPHER L. CASTRO AND HSIN-I CHANG

Department of Atmospheric Sciences, The University of Arizona, Tucson, Arizona

FRANCINA DOMINGUEZ

Department of Atmospheric Sciences, and Department of Hydrology and Water Resources, The University of Arizona, Tucson, Arizona

CARLOS CARRILLO

Department of Atmospheric Sciences, The University of Arizona, Tucson, Arizona

JAE-KYUNG SCHEMM

Climate Prediction Center, NCEP/NWS, Camp Springs, Maryland

HANN-MING HENRY JUANG

Environmental Modeling Center, NCEP/NWS, Camp Springs, Maryland

(Manuscript received 10 August 2011, in final form 18 May 2012)

ABSTRACT

Global climate models are challenged to represent the North American monsoon, in terms of its climatology and interannual variability. To investigate whether a regional atmospheric model can improve warm season forecasts in North America, a retrospective Climate Forecast System (CFS) model reforecast (1982–2000) and the corresponding NCEP–NCAR reanalysis are dynamically downscaled with the Weather Research and Forecasting model (WRF), with similar parameterization options as used for high-resolution numerical weather prediction and a new spectral nudging capability. The regional model improves the climatological representation of monsoon precipitation because of its more realistic representation of the diurnal cycle of convection. However, it is challenged to capture organized, propagating convection at a distance from terrain, regardless of the boundary forcing data used. Dynamical downscaling of CFS generally yields modest improvement in surface temperature and precipitation anomaly correlations in those regions where it is already positive in the global model. For the North American monsoon region, WRF adds value to the seasonally forecast temperature only in early summer and does not add value to the seasonally forecast precipitation. CFS has a greater ability to represent the large-scale atmospheric circulation in early summer because of the influence of Pacific SST forcing. The temperature and precipitation anomaly correlations in both the global and regional model are thus relatively higher in early summer than late summer. As the dominant modes of early warm season precipitation are better represented in the regional model, given reasonable large-scale atmospheric forcing, dynamical downscaling will add value to warm season seasonal forecasts. CFS performance appears to be inconsistent in this regard.

Corresponding author address: Dr. Christopher L. Castro, Department of Atmospheric Sciences, The University of Arizona, Physics and Atmospheric Sciences Bldg., Rm. 520, 1118 East Fourth Street, Tucson, AZ 85721-0081.
E-mail: castro@atmo.arizona.edu

1. Introduction

Official seasonal forecasts for the United States are issued by the National Centers for Environmental Prediction (NCEP) Climate Prediction Center (CPC) within

the National Oceanic and Atmospheric Administration (NOAA). CPC uses a combination of statistical and numerical modeling tools to generate their forecasts (<http://www.cpc.noaa.gov>). These seasonal forecasts are important for natural resource decision making within the United States. In the arid southwest United States, our main geographic area of concern, water resources, agriculture, and ecosystems are particularly sensitive to climate variability (e.g., Cayan et al. 1998; Redmond and Koch 1991; Piechota and Dracup 1996; Piechota et al. 1997). Skillful cool season seasonal forecasts are possible because atmospheric teleconnection responses associated with El Niño–Southern Oscillation (ENSO) can be resolved by global seasonal forecast models (Livezey and Timonfeyeva 2008) and are present as statistically robust features in observational data (e.g., Lau 1985; Ropelewski and Halpert 1986; Held et al. 1989; Tribbia 1991; McCabe and Dettinger 1999; Ropelewski and Halpert 1986; Kiladis and Diaz 1989). Cool season CPC seasonal forecasts are reliable enough to be useful for informing water-related decision making in the western United States (e.g., Schneider and Garbrecht 2005). However, producing skillful operational seasonal forecasts for the warm season, including the North American monsoon system (NAMS), has been more challenging. The warm season is no less important for resource decision making, though, and the main concerns at this time are water demand, severe weather, extreme heat, drought, and wildfire (Ray et al. 2006).

Can the operational modeling component in the CPC seasonal forecasts be potentially improved to provide better NAMS seasonal outlooks? This component presently consists of the Climate Forecast System (CFS) general circulation model at T62 resolution (about 200 km) that generates ensemble members for operational forecasts each month. A CFS reforecast product (1981–2004) has been recently created, with the primary intent to assess the characteristic behavior and biases in the modeling system (Saha et al. 2006). The CFS represents large-scale circulation anomaly patterns well in the winter (e.g., in 200- or 500-mb geopotential height) because of their strong tie to remote Pacific SST forcing. Therefore, CFS has demonstrable skill in forecasting precipitation for the cool season, and the forecasting skill increases when a greater number of ensemble members are used. However, the NAMS in CFS is not represented as a salient climatological feature, even at T126 resolution (Yang et al. 2009). The same is true for GCMs used for climate change projection (Liang et al. 2008). Schemm et al. (2009) demonstrated that an experimental version of the CFS model at T382 resolution, with five ensemble members initialized in late spring for the period 1982–2000, improves NAMS climatology and interannual variability.

To represent the NAMS in a dynamic modeling system, two conditions must be reasonably satisfied. First, the mesoscale physical processes that actually lead to precipitation must be present in the model simulation to some degree. Coarse-resolution GCMs generally have a poor representation of the terrain-forced diurnal cycle of convection (e.g., Collier and Zhang 2007; Lee et al. 2007), which is highly related to the organized convection initiation and the main source of precipitation in the North American monsoon region (Lang et al. 2007; Nesbitt et al. 2008). The likely reasons why GCMs fail to represent it well are because of their poor representation of terrain forcing, mesoscale features (e.g., low-level jets), land–atmosphere coupling, and parameterized convective rainfall. Second, the model should reasonably represent the climatology and interannual variability of the large-scale (or synoptic-scale) circulation during the warm season. Most important for NAMS are the evolution and positioning of a monsoon ridge at mid- to upper levels in the atmosphere, typically viewed at 500 mb (e.g., Castro et al. 2001). As the monsoon ridge develops in Mexico in late spring to early summer and moves north and west into the southwest United States by mid- to late summer, precipitation increases in the southwest and decreases in the central United States (e.g., Higgins et al. 1997; Barlow et al. 1998). The interannual variability of the monsoon ridge is influenced by Pacific SST forcing in early summer (e.g., Castro et al. 2001, 2007b; Grantz et al. 2007), reflected in the dominant mode of early summer U.S. precipitation anomalies (Castro et al. 2009). The observed relationship that wet (dry) winters are typically followed by a dry and delayed (wet and early) summer monsoon in the Southwest is therefore most likely explained by the existence of Pacific SST-associated teleconnections in both the cool and warm seasons (Castro et al. 2007b). Another important consideration is intraseasonal precipitation variability associated with synoptic-scale disturbances (i.e., inverted troughs and easterly waves) and tropical cyclones (e.g., Douglas and Englehart 2007; Bieda et al. 2009; Corbosiero et al. 2009). Severe, organized monsoon thunderstorms require a combination of decreased atmospheric stability, enhanced upper-level divergence and vertical wind shear, and low-level moisture (e.g., Maddox et al. 1995). The resulting “bursts” of precipitation are typically associated with westward propagating mesoscale convective systems originating on the Mogollon Rim or Sierra Madre Occidental (e.g., Bieda et al. 2009).

Dynamical downscaling can be basically classified into four types, according to Castro et al. (2005) and Rockel et al. (2008): type 1, numerical weather prediction; type 2, retrospective historical climate simulation; type 3, seasonal climate forecasting; and type 4, climate change

projection. Castro et al. (2007a,b) used the Regional Atmospheric Modeling System (RAMS) forced with NCEP–National Center for Atmospheric Research (NCAR) reanalysis data in a type 2 dynamical downscaling mode to perform retrospective simulations of the warm season for the period 1950–2002. They basically showed, given “perfect” observed boundary forcing with a reanalysis (type 2 dynamical downscaling), that a regional climate model (RCM) can improve the representation of the NAMS in terms of its climatology and interannual variability. Their results with respect to NAMS climatology are similar to those reported for the North American Monsoon Model Assessment Project (NAMAP; Gutzler et al. 2005) and other long-term simulations from other regional atmospheric models (e.g., Cerezo-Mota et al. 2011). Higher-order, prognostic dynamical downscaling types can thus potentially improve the representation of NAMS from the coarser-resolution driving global model, with two provisos. First, the driving GCM must have a “reasonable” representation of warm season large-scale circulation in terms of climatology and interannual variability (e.g., Pacific SST-associated teleconnection patterns). Second, the RCM must retain the large-scale variability of the driving global model. To accomplish this, interior nudging is needed for the RCM to maintain the amplitude of synoptic-scale features such as ridges and troughs (Castro et al. 2005; Rockel et al. 2008).

This study evaluates the use of the Weather Research and Forecasting model (WRF) to dynamically downscale CFS reforecast data for the period 1982–2000. The primary objective is to demonstrate the potential for an improved NAMS warm season forecast capability, addressing one of the major scientific objectives of North American Monsoon Experiment (NAME; Higgins et al. 2006; Higgins and Gochis 2007). It complements existing efforts within and/or supported by CPC to improve NAM forecasts with both the aforementioned higher T382 resolution of the CFS model and the Regional Spectral Model (RSM), both currently available as experimental real-time products through the North American Monsoon Forecast Forum. A similar study by Chan and Mishra (2011) recently concluded that the RSM is similar to CFS in the representation of NAMS hydroclimate, with problems in the representation of diurnal and seasonal variability. The present work addresses these similar issues with WRF, but with differing conclusions. The paper is organized as follows: Data and methods are described in section 2, including a brief description of WRF, the driving CFS model data, how they are dynamically downscaled, and how the simulations were analyzed and compared with observational proxy data. Section 3 highlights the climatological

performance of the RCM. Anomaly correlations of surface temperature and precipitation and the relative value added of dynamical downscaling for NAMS seasonal forecasting are presented in section 4. Relationships of dominant precipitation modes to Pacific SST variability are shown in section 5. Concluding points and further discussion are in section 6.

2. Data and methods

a. Regional climate model with spectral nudging

The RCM that used is the Advanced Research version of the Weather Research and Forecasting model (ARW-WRF, hereafter WRF), version 3.1 (Skamarock et al. 2005). Similar to other RCMs, WRF is designed primarily to represent mesoscale and cloud-scale atmospheric phenomena. The specific model physical parameterizations used are consistent with those of the existing WRF NWP system at The University of Arizona that produces quasi-operational forecasts for Arizona during the summer at grid spacing of 1.8 km. They include WRF single-moment three-class microphysics (Hong et al. 1998, 2004); Lin microphysics (Lin et al. 1983); Kain–Fritsch cumulus parameterization (Kain and Fritsch 1993; Kain 2004); Goddard shortwave radiation (Chou and Suarez 1994); Rapid Radiative Transfer Model (RRTM) longwave (Mlawer et al. 1997); Eta surface layer (Janjic 1996, 2002); Mellor–Yamada–Janjic (MYJ) planetary boundary layer (Janjic 1990, 1996, 2002); and the Noah land surface model (Ek et al. 2003). RCM simulations are performed for a single grid, contiguous U.S.–Mexico domain at 35-km grid spacing, nearly identical in domain structure to that in Castro et al. (2007a) with similar parameterized physics options.

It is becoming increasingly recognized in the use of RCMs that there is a loss of synoptic-scale variability from the driving GCM when the limited area model is forced only at its lateral boundaries (e.g., Castro et al. 2005; Kanamitsu and Kanamaru 2007). The loss of synoptic-scale variability can then affect how the RCM represents features on the mesoscale, such as convective precipitation (e.g., Castro et al. 2005). An alternative approach to lateral boundary nudging in a buffer zone (e.g., Davies 1976) is spectral nudging, in which selective nudging at only the largest scales takes place throughout the entire domain of the model for prognostic fields (e.g., von Storch et al. 2000). Typically, the nudging is confined to the upper levels of the atmosphere through a weighting function. The variability of the synoptic-scale circulation features may be maintained during the model integration, while allowing the RCM to still add value at the smaller scales and closer to the

surface boundary. RCM simulations that use spectral nudging have been shown to be more realistic in comparison with observations for type 2 dynamical downscaling (e.g., von Storch et al. 2000; Miguez-Macho et al. 2005; Rockel et al. 2008). The spectral nudging method as described in Miguez-Macho et al. (2005), as recently adapted for use in WRF, is used to nudge the model at scales larger than 4 times the grid spacing of the driving global model or reanalysis, approximately 1000 km for T62 resolution. Specifically, the temperature, winds, and geopotential height are nudged.

b. Dynamical downscaling of retrospective seasonal forecasts and global reanalyses

Two types of data are dynamically downscaled. The first is CFS model version 1 ensemble members from the reforecast (Saha et al. 2006) at T62 resolution, and these simulations are henceforth referred to as WRF-CFS. In this study, the base period of 1982–2000 is used to establish a WRF-CFS RCM climatology and evaluate performance of the modeling system. Twice-daily (0000 and 1200 UTC) CFS reforecast data were obtained from the NCEP mass storage system. We had nine ensemble members per year available for dynamical downscaling. These consist of three sets, each initialized from the NCEP global reanalysis at the beginning of the preceding April, May, and June, respectively, as described in Saha et al. (2006). It was not possible to obtain the complete set of CFS ensemble members for each monthly seasonal forecast initialization or the CFS data, and this will adversely affect the statistical robustness of the WRF-CFS simulations. Initial WRF model soil moisture is specified from the North American Regional Reanalysis (NARR; Mesinger et al. 2006). Use of NARR soil moisture helps to minimize the problematic soil moisture spinup issue in RCM simulations (e.g., Liston and Pielke 2000) as both NARR and our WRF simulations use the identical land surface model (Noah) and roughly equivalent spatial resolution. As will be shown, CFS data used for the downscaling are adequate to address the question of whether WRF can improve upon the CFS model representation of climatology and interannual variability, thus evaluating the utility of type 3 dynamical downscaling for the North American monsoon.

The WRF-CFS simulations are compared with equivalent type 2 dynamical downscaling using the NCEP–NCAR reanalysis as boundary forcing. These simulations henceforth referred to as WRF–NCEP. The WRF–NCEP simulation is identical in principle to those described in Castro et al. (2007a) with RAMS. The major difference is the WRF–NCEP simulation is a continuous integration starting from the beginning of 1979 (or start of NARR) through 2000, also initialized with NARR soil moisture.

We note that the NCEP–NCAR reanalysis may not be the best quality reanalysis for the type 2 dynamical downscaling. Cerezo-Mota et al. (2011) dynamically downscaled both the 40-yr European Centre for Medium-Range Weather Forecasts (ECMWF) Re-Analysis (ERA-40) and the NCEP–NCAR reanalysis data with the Hadley Centre Regional Model version 3 with Providing Regional Climates for Impacts Studies (PRECIS) physics (HadRM3P) in the North American monsoon region. They demonstrated that model simulated precipitation in an Arizona–New Mexico region was adversely impacted by a large deficit of moisture in the Gulf of Mexico in those simulations using the NCEP–NCAR reanalysis as boundary forcing, at least in the context of their RCM simulation design. However, they also concluded that either downscaled reanalysis appropriately captured monsoon interannual variability. This latter conclusion is consistent with the analysis of NAMS interannual variability in the RAMS simulations with NCEP–NCAR reanalysis boundary forcing described in Castro et al. (2007b), and thus provides the justification for the similar type 2 dynamical downscaling experiments done here with WRF. It is actually the more relevant conclusion from Cerezo-Mota et al. (2011) that bears on this work, since seasonal predictability is strongly linked to Pacific SST forcing, as we will show later.

c. Observational proxy data for model performance evaluation

Several commonly and widely available observational proxy data products are used to compare with GCM and RCM simulations, mostly consistent with Saha et al. (2006). The NCEP–NCAR reanalysis (Kalnay et al. 1996) is used for comparison of large-scale circulation fields in the CFS global model simulation in terms of 500-mb geopotential height. Spectral nudging ensures these fields are nearly identical in the RCM. Observed surface temperature data are from the University of Delaware (UDeI) dataset at a resolution of 0.5° (Shepard 1968; Willmott et al. 1985; Legates and Willmott 1990; Willmott and Matsuura 1995), and these are compared with the 2-m surface air temperature generated by WRF. Observed precipitation data are considered with a new National Oceanic and Atmospheric Administration (NOAA)-developed precipitation dataset (P-NOAA) at 0.5° resolution that covers all of North America, provided to us by Drs. Russ Vose and Ed Cook. P-NOAA is similar to the Precipitation-Elevation Regressions on Independent Slopes Model (PRISM) product (Daly et al. 1994), which considers the dependence of elevation on precipitation. Gridded precipitation fields were developed using data from 12 710 precipitation stations. U.S. and Canadian data were from their respective national

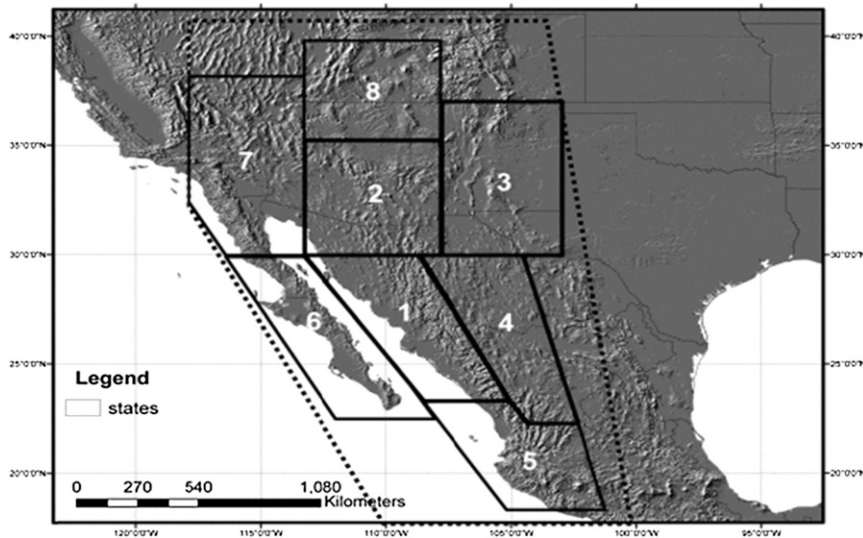


FIG. 1. NAME precipitation zones (1–8), as originally shown in the final report of the 10th NAME Science Working Group Meeting.

archives (the National Climatic Data Center, the Mexican Meteorological Service, and Environment Canada). Climatologically aided interpolation was applied to interpolate the irregularly spaced station data into $0.5^\circ \times 0.5^\circ$ grid spacing data using latitude, longitude, and elevation as predictors, and involves inverse distance weighting approach for computing precipitation and temperature anomalies (Willmott et al. 1985; Willmott and Matsuura 1995; Hutchinson et al. 2009). To compute anomaly correlations, both model simulated and proxy observed temperature and precipitation have been normalized at each grid point on their respective grids. The normalization of temperature simply considers a normal distribution for a defined time period. Precipitation anomalies are defined using the standardized precipitation index (SPI; McKee et al. 1993). The SPI technique transforms a given precipitation anomaly into a normalized value, assuming the distribution of precipitation for a defined period fits a gamma distribution. The parameters of the gamma distribution (α and β) for CFS and WRF-CFS precipitation are computed from the climatological base period of 1982–2000, and for WRF-NCEP precipitation using the climatological base period of 1979–2000. SPI normalizes the precipitation data to implicitly account for precipitation bias in a given modeling system when comparing results to observations, accounting for the typical nonnormality of precipitation distributions. Castro et al. (2009) showed that the dominant spatial patterns in observed warm season SPI in North America have strong statistical relationships with Pacific SST forced atmospheric teleconnections, the principal driver of NAMS variability in summer.

Dominant modes of SPI variability are determined using rotated EOF (REOF) analysis (e.g., Richman 1986) and these are linearly regressed on large-scale atmospheric circulation anomalies and global sea surface temperature anomalies.

d. Anomaly correlations at each grid point and NAME precipitation zones

A Pearson correlation (e.g., Wilks 2006) of the observed and model-simulated precipitation and surface temperature anomalies is considered for early summer [June–July (JJ)] and late summer [August–September (AS)] periods for the entire regional model domain of the contiguous United States and Mexico. As mentioned, the teleconnectivity of the NAMS to Pacific SSTs diminishes in the late summer, so the consideration of the traditional three-month average [June–August (JJA)], as is customary in the current NCEP seasonal forecast operational products, would tend to wash out any potentially predictive Pacific SST signal on early warm season precipitation. Before the computation of the anomaly correlation, observed proxy temperature and precipitation data have been regridded to the native resolution of the GCM or RCM, as this much better highlights the impact of enhanced resolution of the terrain in the RCM and any associated value added. The resolution of the RCM and the observed temperature and precipitation data are roughly the same, so there is little impact of the regridding on the computation of anomaly correlations at the RCM grid spacing of 35 km. Subregional precipitation zones were defined consistent with those used in the NAME Forecast Forum (Fig. 1).

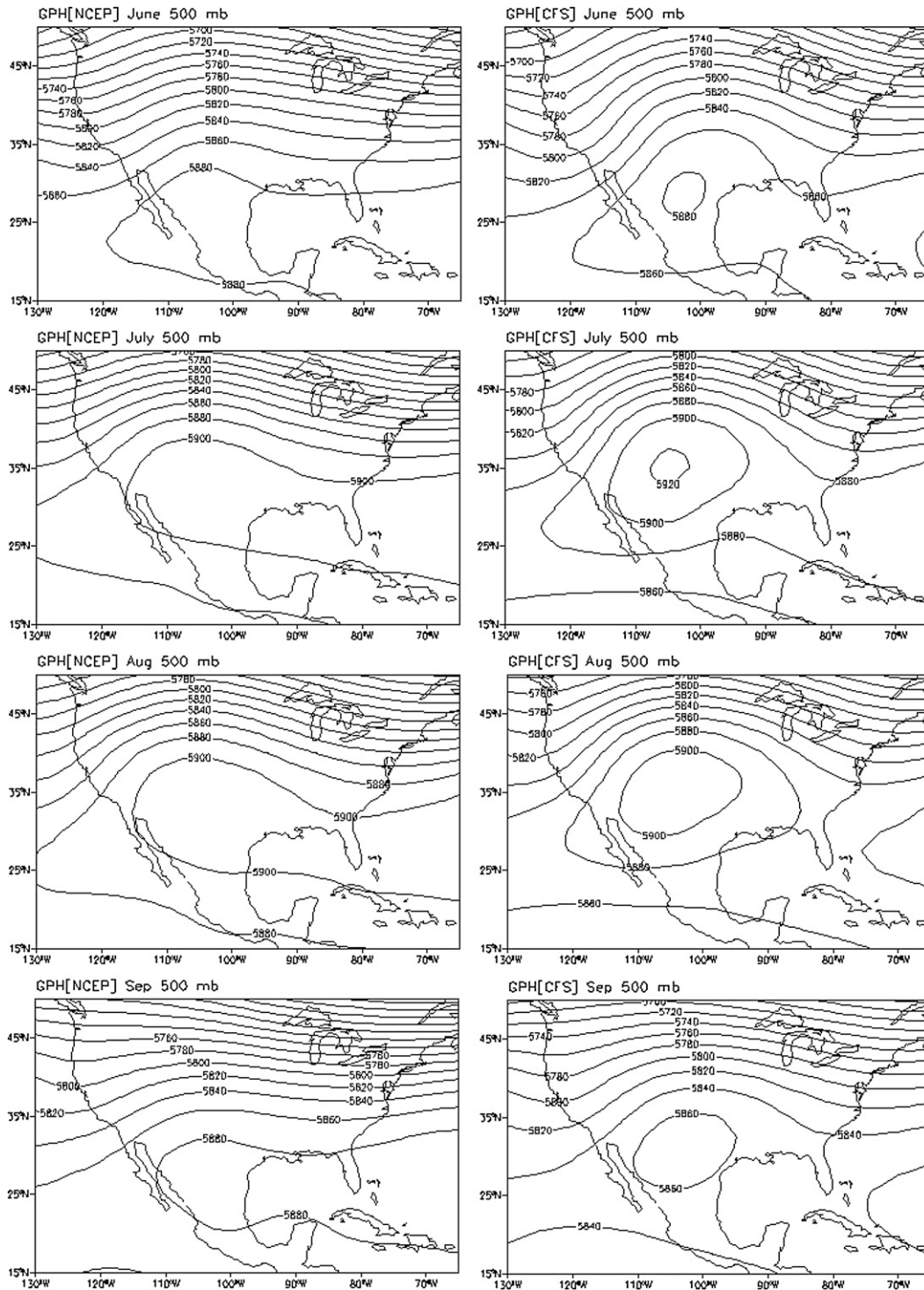


FIG. 2. Monthly average 500-mb geopotential height (m) for the period June through September from the NCEP-NCAR reanalysis and nine-member CFS ensemble (1982–2000). Contour interval is 20 m.

These zones roughly reflect the regional-scale contrasts in the climatology and interannual variability of NAMS precipitation (e.g., Comrie and Glenn 1998). The core monsoon region, which exhibits the classical NAMS

climatological characteristics and where most observational data was collected during NAME, includes the following zones: 1) approximately central Sonora and Sinaloa extending eastward to the crest of the Sierra

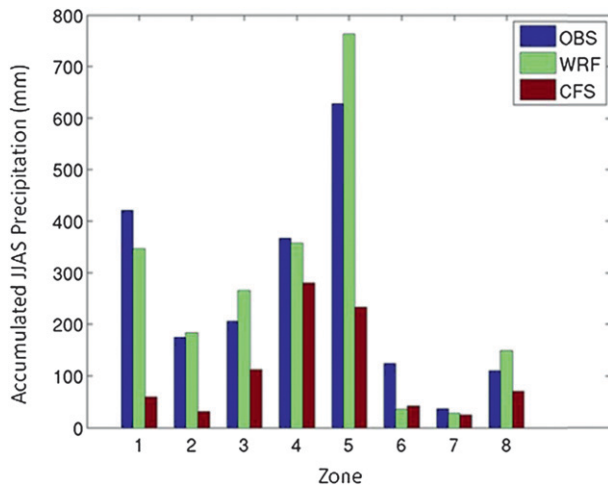


FIG. 3. Average annual warm season (JJAS) accumulated precipitation (mm) in the NAME precipitation zones for the period 1982–2000, considering CPC observed precipitation (blue), CFS GCM model (dark red), and WRF dynamically downscaled CFS ensemble members (light green).

Madre Occidental and 2) northern Sonora and most of southern Arizona. Owing to their location west of the Continental Divide, these two zones have the same response in the interannual variability of warm season

precipitation in relation to Pacific SST variability, with typically a weaker and later (stronger and earlier) monsoon precipitation during El Niño and a positive phase of Pacific decadal variability (PDV) (La Niña, negative PDV) conditions (see Castro et al. 2007b, their Fig. 8). The anomaly correlation for the eight NAME precipitation zones is determined as the spatial average of the anomaly correlation maps within the given area.

3. Highlights of warm season climatology in WRF-CFS simulations

Before considering seasonal forecast performance of CFS versus WRF-CFS, it is necessary to first establish if the seasonal forecast RCM simulations adds value in terms of representing the climatology of the NAMS. We present some highlighted results to demonstrate the improved representation of precipitation in the RCM, consistent with Castro et al. (2007a). Figure 2 shows the monthly evolution of the monsoon ridge at 500 mb in the NCEP reanalysis and CFS model ensemble members for the period June to September. Both reanalysis and CFS show a well-defined monsoon ridge that develops in June in northern Mexico, advances north and westward toward the southwestern

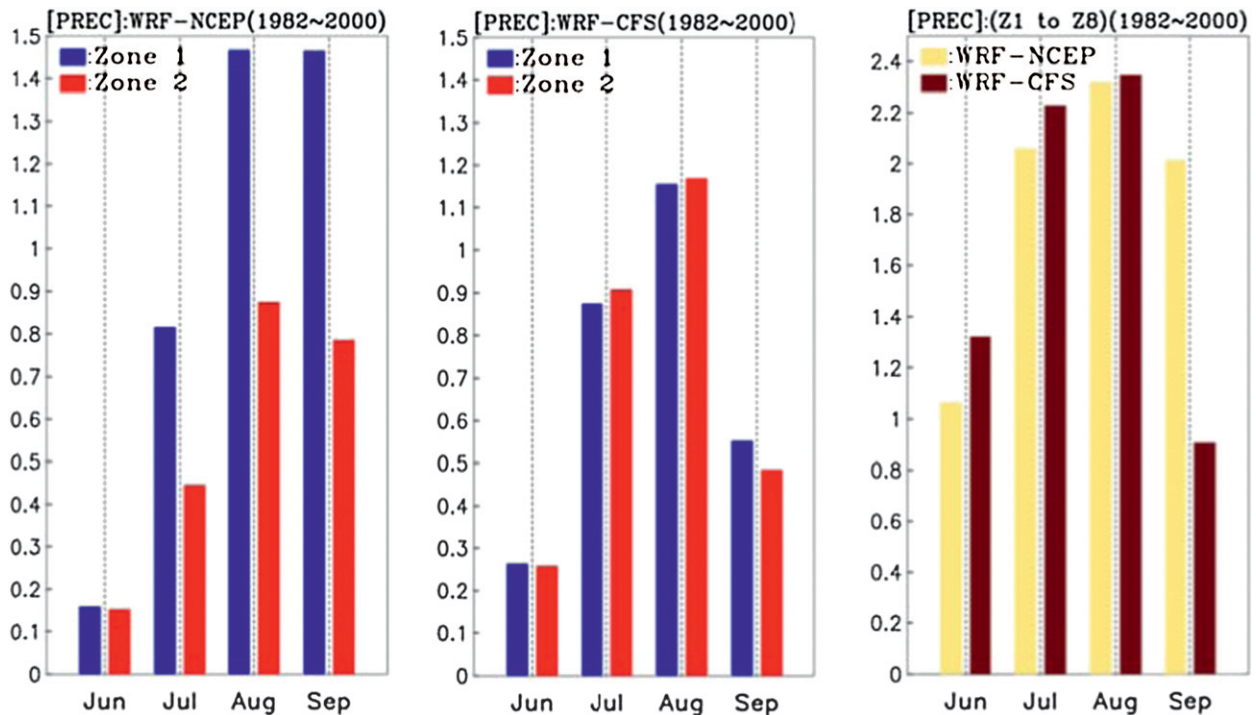


FIG. 4. Monthly average precipitation (mm day^{-1}) during the warm season (JJAS) for the period 1982–2000, considering (left) WRF-NCEP and (middle) WRF-CFS for NAME precipitation zones 1 and 2 of the core monsoon region. (right) Same information considering all NAME precipitation zones.

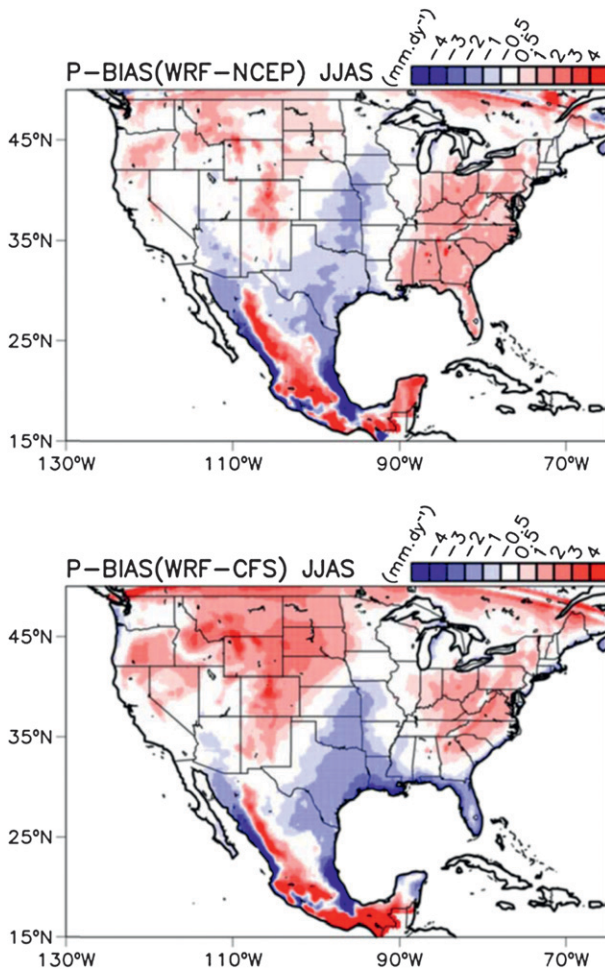


FIG. 5. Average warm season (JJAS) precipitation bias (mm day^{-1}) for (top) WRF-NCEP and (bottom) WRF-CFS ($\text{P-BIAS} = \text{RCM} - \text{P-NOAA}$ observation). Red (blue) colors indicate precipitation overestimation (underestimation) by WRF.

United States in July and August, and then retreats back into Mexico by September, similar to Castro et al. (2001, their Fig. 6). Although the CFS model gives a good representation of the climatology of the large-scale circulation, it has a poor representation of NAMS rainfall. The annual warm season [June–September (JJAS)] average precipitation for the NAME precipitation zones is shown in Fig. 3. CFS consistently underestimates NAMS precipitation overall, but especially so in zones 1 and 2, as the CFS precipitation only produces 10%–20% of the actual total in Sonora and Arizona. WRF-simulated precipitation is much improved, and quite close to the climatological value of about 200 mm in zone 2. The average monthly precipitation rate for the core monsoon region and all NAME precipitation zones (Fig. 4) shows the expected rapid increase in precipitation in both WRF-NCEP and WRF-CFS during monsoon

onset from June to July, although their precipitation totals slightly differ during July and August. Figure 5 shows the RCM-simulated climatological precipitation bias for WRF-NCEP and WRF-CFS. Both types 2 and 3 WRF dynamical downscaling overestimate precipitation directly over complex terrain, such as the Rocky Mountains or Sierra Madre. Precipitation is underestimated in zones where more organized, propagating convection accounts for the majority of warm season rainfall, such as west of the Sierra Madre or east of the Rockies in the southern Great Plains (e.g., Carbone et al. 2002). As mentioned, it has been noted that the NCEP reanalysis may underestimate atmospheric moisture over the Gulf of Mexico (Cerezo-Mota et al. 2011), which may contribute to the negative precipitation bias in the central United States in the type 2 simulation. Since the same problem exists in the type 3 simulation, though, it may also reflect a weakness of the regional model to represent the organized convection that is independent of the boundary forcing data. As we will discuss later, the problem can be alleviated with a modified convective trigger function in the Kain–Fritsch convective parameterization. The representation of mesoscale convective systems downwind of complex terrain appears to be a systematic deficiency of RCMs at this spatial scale (e.g., Gao et al. 2007) and will necessarily affect how it represents interannual precipitation variability, as we will show in the next section.

The RCM is able to add value to the simulation of NAMS precipitation because it improves the representation of physical processes on the mesoscale. The diurnal cycle of convection is caused by the differential heating and cooling of the mountains, as compared to the surrounding atmosphere, drawing air up mountain slopes and forming convective clouds over the mountain tops. Figure 6 shows the diurnal cycle of precipitation (mm h^{-1}) for early (JJ) and late (AS) summer, respectively, at the four RCM output times of 0000, 0600, 1200, and 1800 UTC. In the western United States and Mexico, precipitation correctly peaks in the mid- to late afternoon (1800–0000 UTC), is generally more intense at higher elevation, and increases during late summer. There is also a noticeable maximum in nighttime precipitation in the northern Great Plains (0600 UTC), correctly reflecting the presence of the more organized convection there (e.g., Carbone et al. 2002). Figure 7 shows the monthly evaluation of the average low-level moisture flux (below 850 mb) in WRF-CFS. The Great Plains low-level jet is strongest in the early part of the summer and then decreases in strength in August, and the regional model shows the extension of the low-level jet into the Gulf of Mexico and Caribbean, similar to Castro et al. (2007a, their Fig. 8). Moisture flux in the

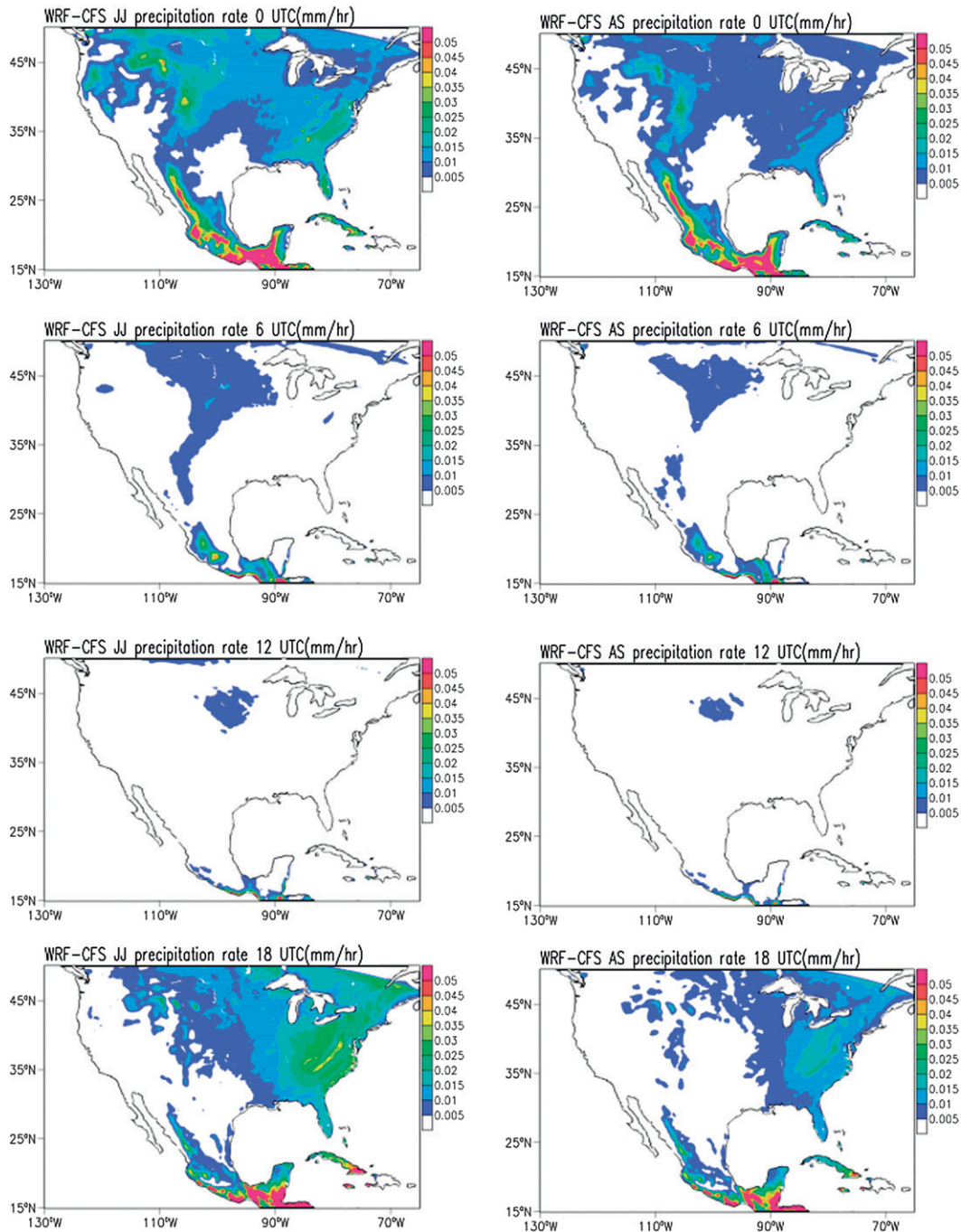
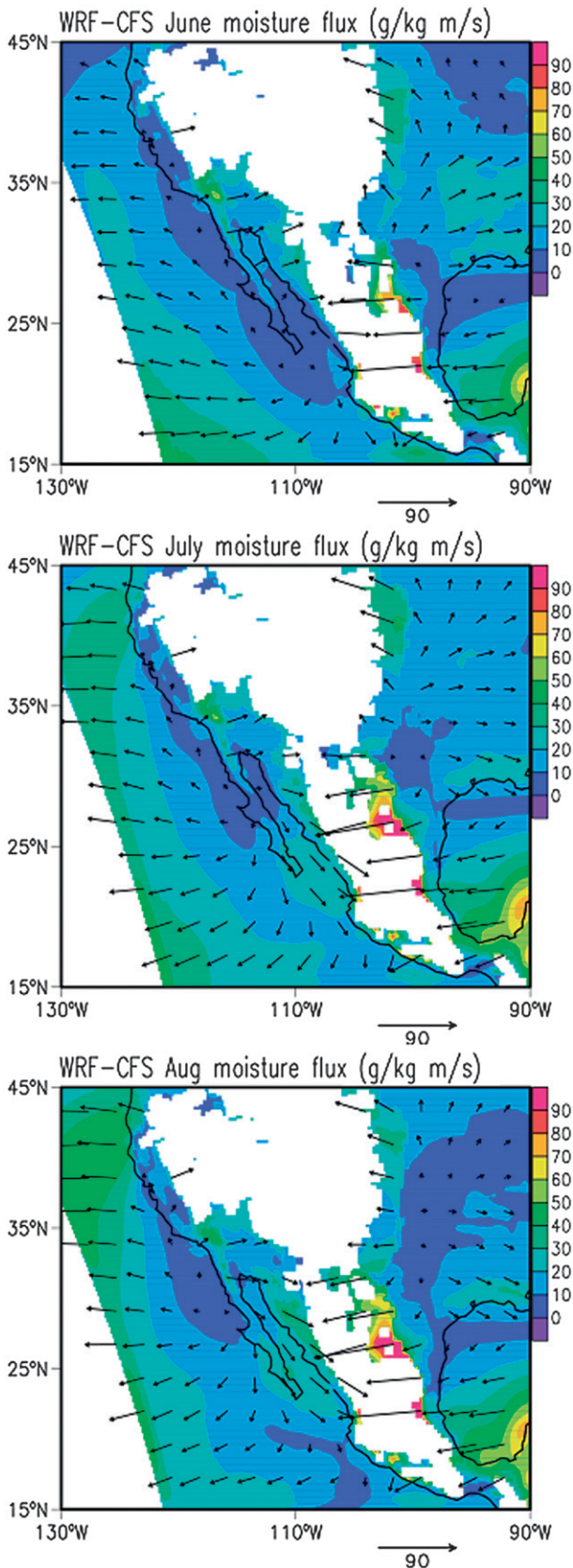


FIG. 6. Average precipitation rate (mm h^{-1}) in WRF-CFS simulations in (left) early (JJ) and (right) late summer (AS) for 0000, 0600, 1200, and 1800 UTC, as labeled.

zones 1 and 2 increases in late summer with the advance of the monsoon, but this moisture flux appears to be associated mainly with the diurnal cycle of convection along the Sierra Madre Occidental, as the monthly average moisture flux vectors are oriented more perpendicular, and not parallel, to the coast in northern Mexico and there is not a local maximum in moisture

flux centered in the Gulf of California. The incorrect representation of Gulf of California low-level jet, coupled with the problems in representing precipitation that occurs farther away from complex terrain as shown in Fig. 5, demonstrates an inability of WRF-CFS to adequately capture the sources of synoptic-scale intra-seasonal variability that would cause moisture surges



in Gulf of California and outbreaks of severe organized NAMS convection. A similar deficiency has been reported for the high-resolution experimental CFS T382 simulations and also exists in the WRF-NCEP simulations (not shown).

4. Temperature and precipitation anomaly correlations: Early versus late warm season

Given that the use of a regional model improves the climatological representation of the NAMS from the driving global CFS model, does it also improve on the anomaly correlation of temperature and precipitation? As mentioned, the anomaly correlations (σ_{anom}) are considered for the early part (JJ) and late part (AS) of the warm season, as it is known a priori that precipitation variability behaves very differently with respect to Pacific SST forcing as the summer progresses. In this section σ_{anom} includes the original reanalysis and CFS model and the corresponding type 2 and type 3 dynamically downscaled WRF results. We show the temperature and precipitation anomaly correlations (σ_{anomT} and σ_{anomP}) respectively in Figs. 8 and 10, considering early summer (JJ) versus late summer (AS); Figs. 9 and 11 show the difference in σ_{anomT} and σ_{anomP} , respectively, between the driving reanalysis or global model and the dynamically downscaled WRF model products. The differences in σ_{anom} (or $\Delta\sigma_{\text{anom}}$) in these figures are gridded to both the resolution of the global model and the regional model, for comparison. Figure 12 shows the same information for precipitation as Figs. 9 and 11, zooming in on the NAME tier 2 region. For reference, a locally statistically significant σ_{anom} at the 90% level, using a t test, is approximately 0.37 or greater.

The values of σ_{anomT} for the NCEP reanalysis and WRF-NCEP, not surprisingly, are high (above 0.6) nearly everywhere in the model domain throughout the warm season, except in central Mexico probably owing to uncertainties in the UDel dataset with elevation (top and lower middle panels in Fig. 8). There is very little difference in σ_{anomT} between NCEP and WRF-NCEP (panels in top two rows of Fig. 9). Considering CFS in JJ (upper middle panel on left), the highest σ_{anomT} occurs in the Southwest. The RCM generally tends to retain or improve on σ_{anomT} in those locations where it is already positive in CFS and worsens it where it is already

FIG. 7. Monthly average integrated low-level moisture flux ($\text{g kg}^{-1} \text{m s}^{-1}$) from surface to 850 mb from WRF-CFS simulations. Vector length and magnitude of moisture flux as indicated.

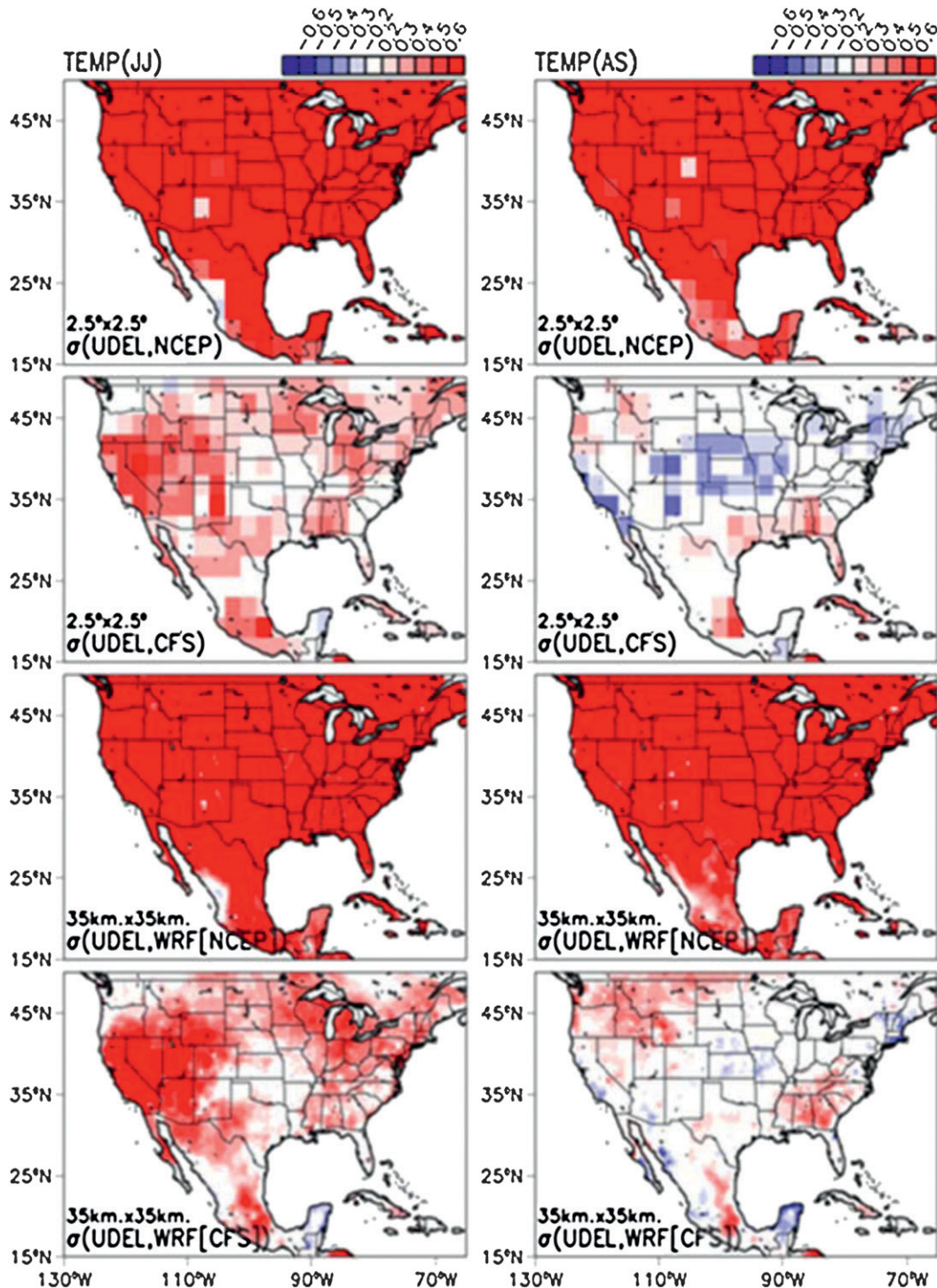


FIG. 8. Anomaly correlation of normalized temperature (σ_{anomT}) for (left) early (JJ) and (right) late summer (AS). Normalized observed UDEL temperature anomalies correlated with those from corresponding (top) NCEP–NCAR reanalysis, (upper middle) CFS model, (lower middle) WRF–NCEP, and (bottom) WRF–CFS. The magnitude of σ_{anomT} is indicated by the color bar. Results shown at native model resolution indicated on the plots.

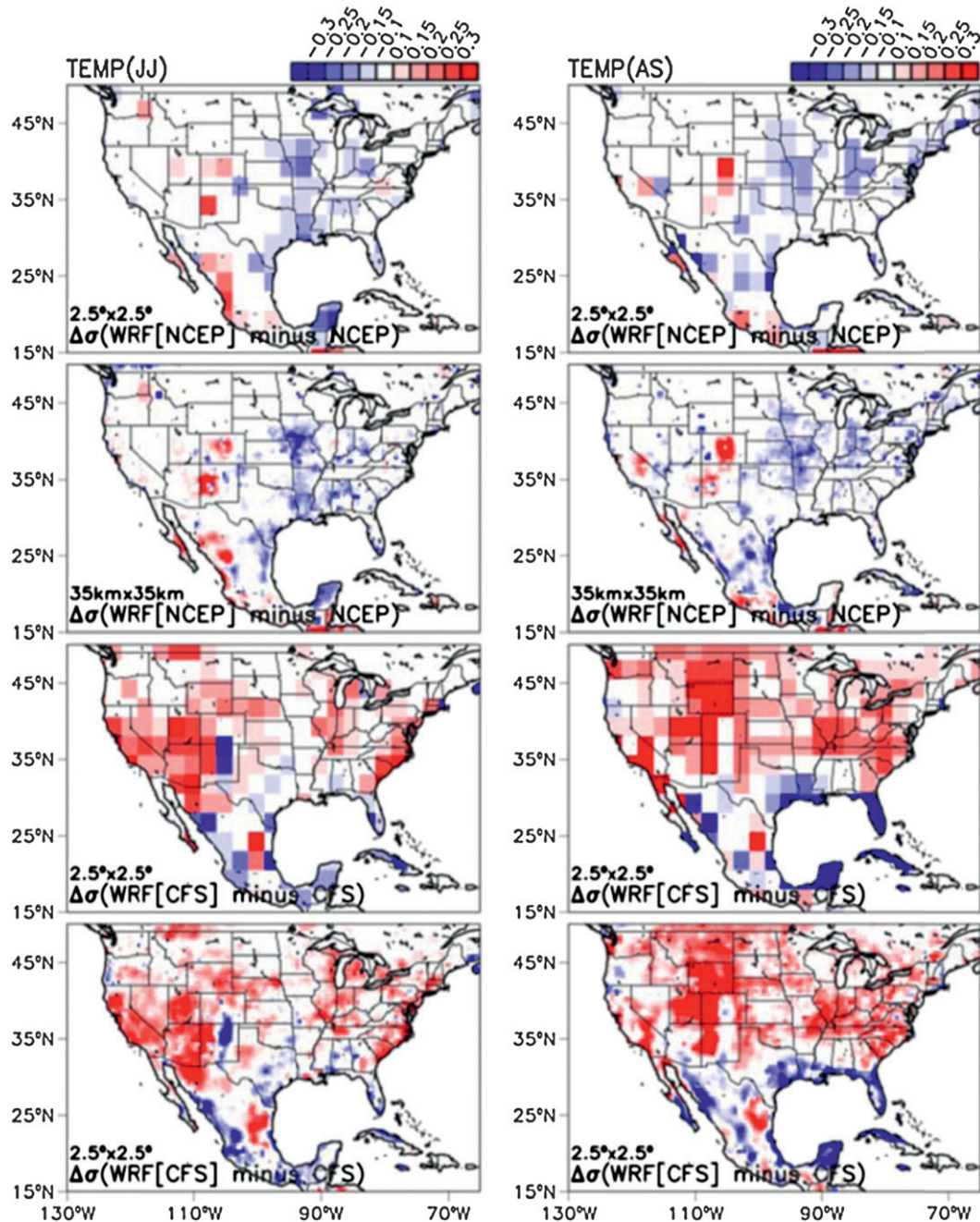


FIG. 9. (top),(upper middle) WRF-NCEP minus NCEP difference in σ_{anomT} for (left) early (JJ) and (right) late summer (AS), gridded to the respective resolutions of each data. (bottom middle),(bottom) As above, but for WRF-CFS minus CFS.

negative in CFS (bottom row of panels of Fig. 8 and bottom two rows of panels in Fig. 9). However, owing to the use of spectral nudging, the continental-scale spatial pattern of σ_{anomT} does not change much in the RCM. During AS, σ_{anomT} is generally much lower everywhere in CFS, and even negative in the central United States (upper middle panel on right in Fig. 8). Notably, the

statistically significant JJ σ_{anomT} present in the Southwest vanishes during AS. Although the AS RCM σ_{anomT} is also worse than JJ, it is still improved from CFS, especially in the northern Rockies and the Southeast.

Values of σ_{anomP} for early versus late summer are considered in Fig. 10. Dynamical downscaling of the NCEP reanalysis tends to increase σ_{anomP} overall within

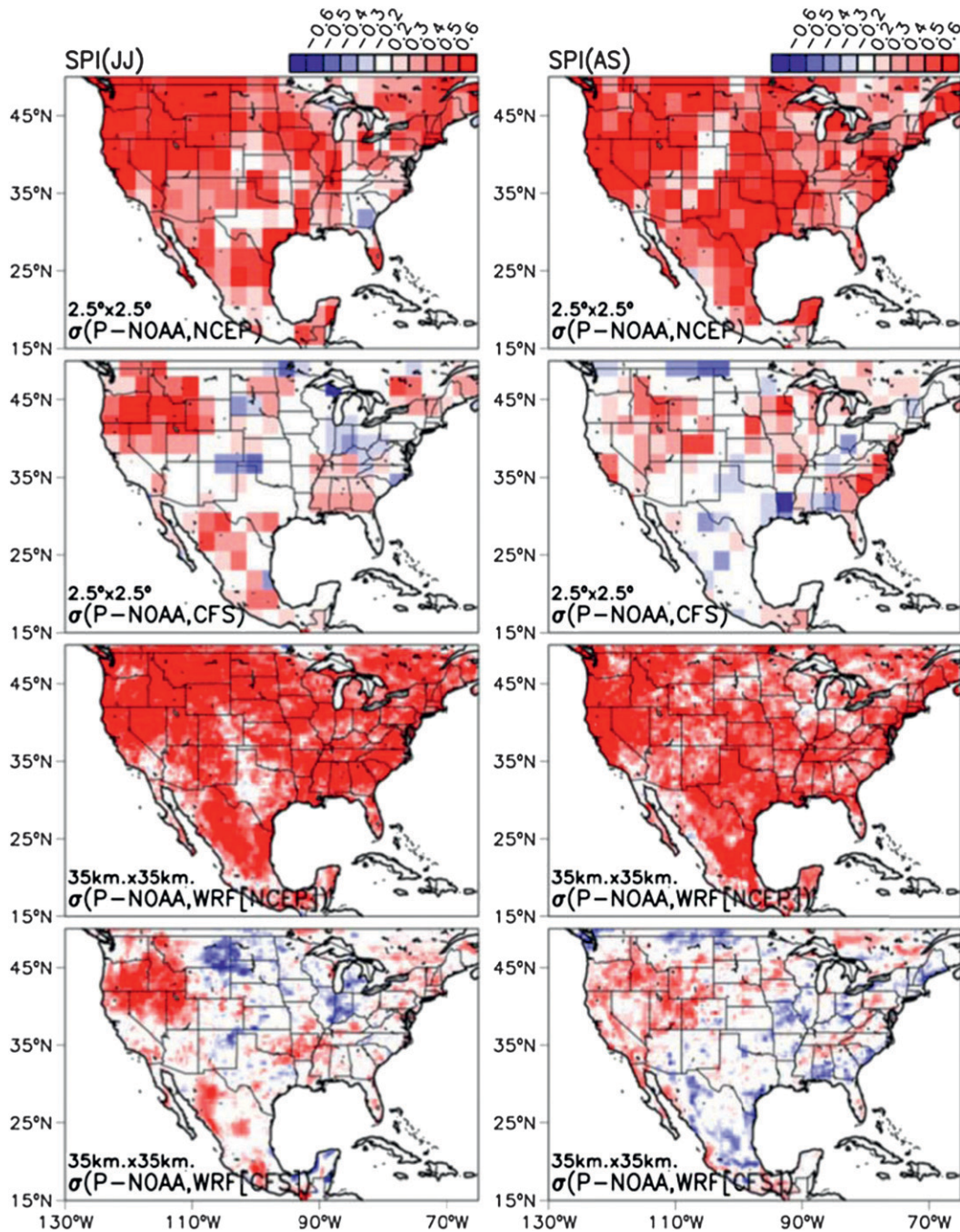


FIG. 10. As in Fig. 8, but for σ_{anomP} for early and late summer. Observed SPI derived from P-NOAA data.

the regional model domain, at least in the early part of the warm season (upper panels in Fig. 11). Zooming in on the NAME tier 2 region (Fig. 12), the highest relative σ_{anomP} in the WRF-NCEP simulations occurs on the crest of the mountains, such as the Mogollon Rim in Arizona (in range of 0.2 to 0.4) and Sierra Madre Occidental in northwestern Mexico (greater than 0.6), and

the regional model increases σ_{anomP} in these areas. The value of σ_{anomP} then decreases rapidly in the lowland desert regions toward the Colorado River valley and Gulf of California, becoming worse than NCEP. The spatial differences in σ_{anomP} in the WRF-NCEP simulations have a very important implication for higher orders of dynamical downscaling such as seasonal forecasting.

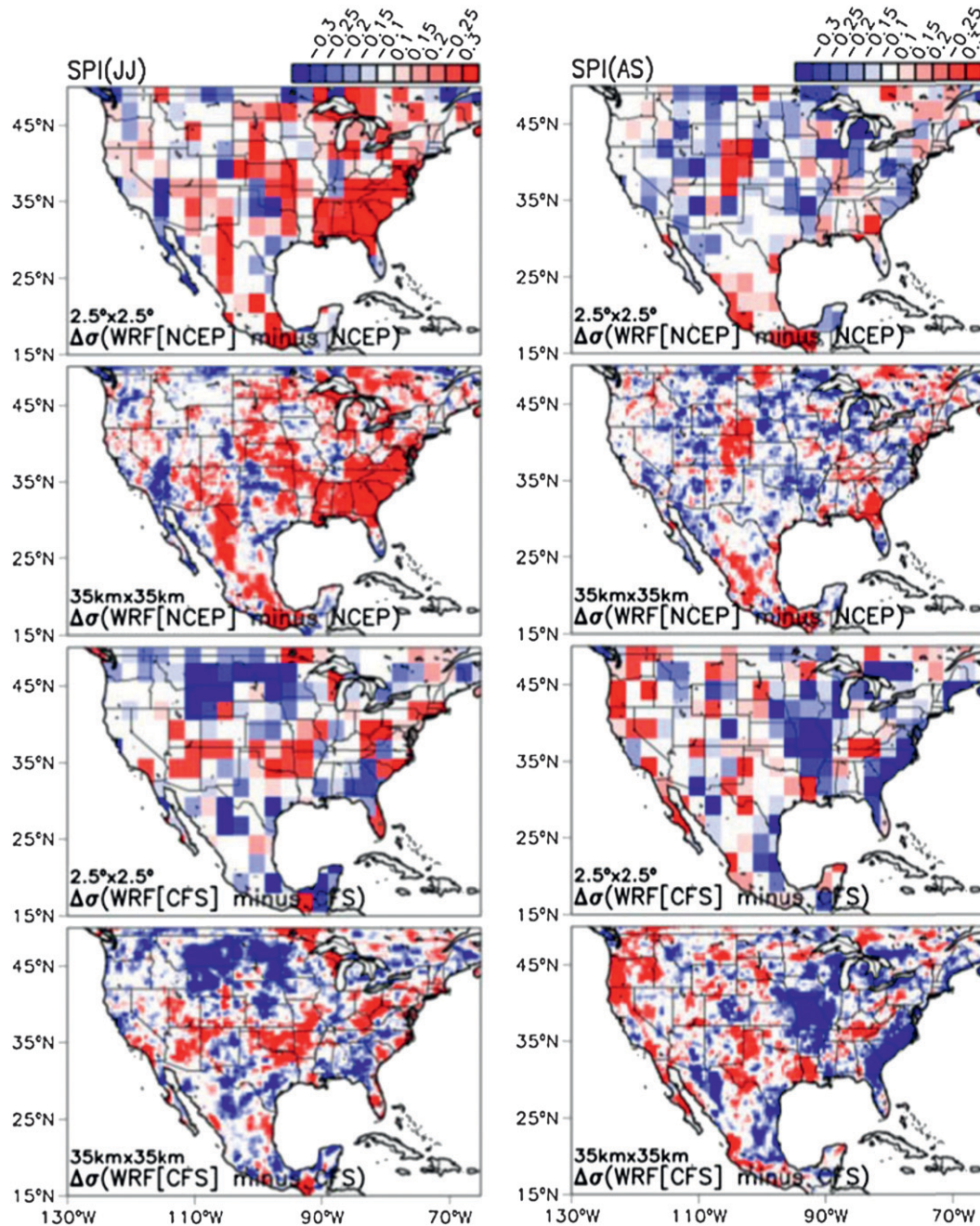


FIG. 11. As in Fig. 9, but for σ_{anomP} for early and late summer.

Even downscaling “perfect” observations from an atmospheric reanalysis, the RCM at 35-km grid spacing is still challenged to represent the interannual variability of organized, propagating convection that causes the majority of monsoon precipitation away from complex terrain, consistent with Gao et al. (2007).

Comparing σ_{anomP} for CFS versus WRF-CFS (upper middle and lower panels, respectively, in Fig. 10), like

for σ_{anomT} , the RCM generally tends to retain or slightly increase σ_{anomP} where it is already of positive sign in CFS and worsen it where it is already of negative sign in CFS. Also, the continental-scale spatial pattern of the σ_{anomP} in WRF-CFS is consistent with CFS. Considering the NAME tier 2 region in Fig. 12, as with WRF-NCEP the highest values of σ_{anomP} in WRF-CFS occur in association with complex terrain in JJ, along

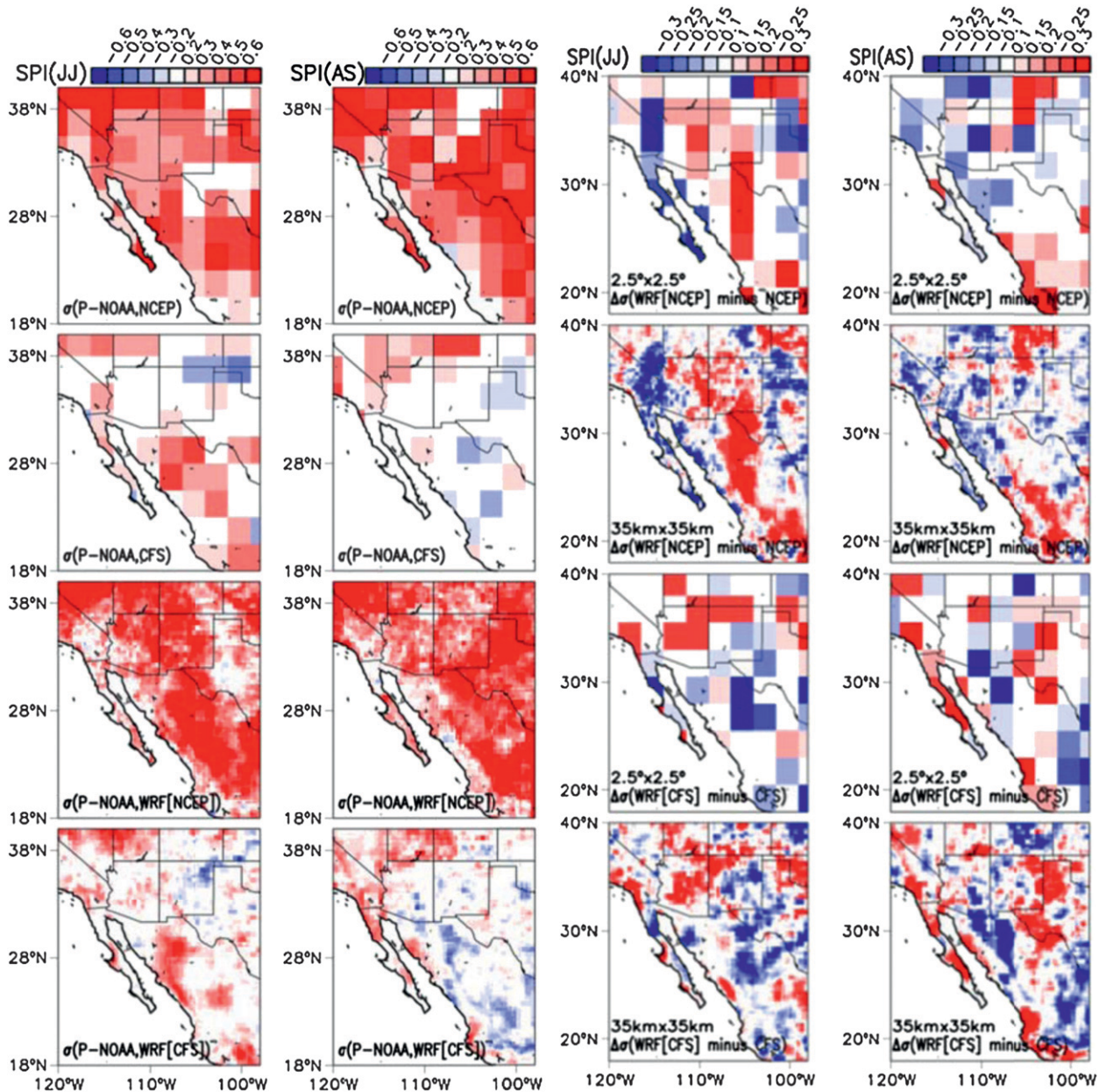


FIG. 12. (left),(middle left) As in Fig. 10, but considering the same geographic areas considered in Fig. 1, corresponding to the NAME tier 2 region. (middle right),(right) As in Fig. 11, but for the NAME tier 2 region.

the crest of the Sierra Madre Occidental and Mogollon Rim in Arizona, and they rapidly decrease westward away from the terrain. The largest increases in σ_{anomP} in WRF-CFS in the tier 2 region occur west of the continental divide in Arizona during JJ. That strongly contrasts with areas east of the continental divide in New Mexico, where WRF-CFS worsens the σ_{anomP} . Outside of the NAMS region, the highest σ_{anomP} in JJ occurs in the northern Great Basin, though there is little difference between CFS and WRF-CFS.

In AS, the positive σ_{anomP} in the NAMS tier 2 region quickly deteriorates from JJ, reflecting the large difference in potential NAMS predictability from the early to late part of the warm season. Values of σ_{anomP} in CFS and WRF-CFS also generally decrease elsewhere.

The early and late summer σ_{anomT} and σ_{anomP} are shown for the NAME precipitation zones in Tables 1 and 2, consistent with Figs. 8 and 10. Values of σ_{anomT} and σ_{anomP} that are statistically significant at the 90%

TABLE 1. Early summer (JJ) and later summer (AS) temperature anomaly correlations (σ_{anomT}) for NAME precipitation zones, considering NCEP, WRF-NCEP, CFS, and WRF-CFS. Statistically significant correlations at the 90% level are in bold shading. For WRF simulations, an asterisk indicates that the dynamically downscaled result is statistically significant and better than the driving coarser-resolution data; boldface indicates that the dynamically downscaled result is worse than the driving coarser-resolution data and statistical significance is retained; and a superscript X indicates that the dynamically downscaled result is worse than the driving coarser-resolution data and statistical significance is lost.

NAME precipitation zones: Early summer (JJ) temperature anomaly correlations				
	NCEP	WRF-NCEP	CFS	WRF-CFS
Zone 1	0.48	0.45	0.17	0.11
Zone 2	0.84	0.85*	0.33	0.53*
Zone 3	0.72	0.79*	0.36	0.39*
Zone 4	0.45	0.61*	0.26	0.24
Zone 5	0.10	0.43*	0.23	0.13
Zone 6	0.45	0.49*	0.38*	0.33 ^X
Zone 7	0.83	0.87*	0.44*	0.55*
Zone 8	0.87	0.90*	0.45*	0.66*

NAME precipitation zones: Late summer (AS) temperature anomaly correlations				
	NCEP	WRF-NCEP	CFS	WRF-CFS
Zone 1	0.51	0.40	0.09	-0.07
Zone 2	0.84	0.82	-0.12	-0.07
Zone 3	0.74	0.80*	-0.11	0.03
Zone 4	0.66	0.61	0.11	0.00
Zone 5	0.36	0.37*	-0.18	-0.14
Zone 6	0.20	0.26	0.11	0.05
Zone 7	0.83	0.81	-0.27	0.08
Zone 8	0.86	0.83	-0.08	0.07

level are denoted in bold shading. We consider the RCM to add value if the RCM σ_{anom} is greater than that of the driving global model and a statistically significant σ_{anom} is retained (denoted with an asterisk); neither add value or take away value if σ_{anom} of the RCM is less than that of the driving global model, but its statistical significance is retained (shown in boldface); and take away value if σ_{anom} of the RCM is both less than that of the driving global model and statistical significance is lost (denoted with a superscript X). Considering temperature in Table 1, WRF-NCEP adds or retains value for all of the NAME zones in early and late summer. WRF-CFS adds value to σ_{anomT} in four of the eight zones in early summer, including zone 2 (Arizona) in the core monsoon region, and only takes away value in zone 6 (Baja California). In late summer (AS), there is no statistically significant σ_{anomT} in either CFS or WRF-CFS in any of the NAME zones. Considering precipitation, WRF-NCEP adds or retains value in four of the

TABLE 2. As in Table 1, but for anomaly correlation of early and late summer precipitation (σ_{anomP}).

NAME precipitation zones: Early summer (JJ) SPI anomaly correlations				
	NCEP	WRF-NCEP	CFS	WRF-CFS
Zone 1	0.48	0.29 ^X	0.09	0.23
Zone 2	0.43	0.37	0.07	0.13
Zone 3	0.40	0.57*	-0.04	0.03
Zone 4	0.45	0.68*	0.40	0.29
Zone 5	0.15	0.26	0.23	0.19
Zone 6	0.17	0.19	0.11	0.09
Zone 7	0.38	0.26 ^X	-0.05	0.11
Zone 8	0.58	0.56	0.18	0.20

NAME precipitation zones: Late summer (AS) SPI anomaly correlations				
	NCEP	WRF-NCEP	CFS	WRF-CFS
Zone 1	0.33	0.23	0.06	0.10
Zone 2	0.41	0.35 ^X	0.10	-0.03
Zone 3	0.46	0.51*	-0.02	-0.04
Zone 4	0.39	0.48*	0.04	-0.16
Zone 5	0.01	0.34	-0.12	-0.04
Zone 6	0.37	0.40*	0.06	0.10
Zone 7	0.54	0.26 ^X	0.33	0.36
Zone 8	0.56	0.46	0.24	0.26

eight NAME zones. For the core monsoon region zones 1 and 2, WRF-NCEP consistently has a lower σ_{anomP} than NCEP throughout the warm season. This loss of value likely reflects the failure of the regional model to represent organized, propagating convection west of the Sierra Madre and Mogollon Rim, as we discussed earlier in reference to Fig. 12. WRF-CFS precipitation is not adding value above that of CFS for any of the NAME zones throughout the summer, by our criteria. It is worth noting, though, that there are slight improvements in the σ_{anomP} in the core monsoon region (zones 1 and 2) in early summer. The performance of WRF-CFS RCM is qualitatively similar to the high-resolution experimental T382 CFS reported in Schemm et al. (2009) for NAME precipitation zones. They noted slight improvements in σ_{anomP} from T126 resolution, especially in those zones where it was already of positive sign in the coarser model, and a general decrease in σ_{anomP} in late summer. The SPI time series used to compute the precipitation anomaly correlation for zones 1 and 2 (Fig. 13) shows that forecast SPI anomaly of WRF-CFS is highly correlated with CFS (0.78 for zone 1 and 0.56 for zone 2). So the RCM modulates the magnitude of the forecast precipitation anomaly from the global model, but does not change the large-scale circulation patterns that would lead to abnormally wet or dry conditions.

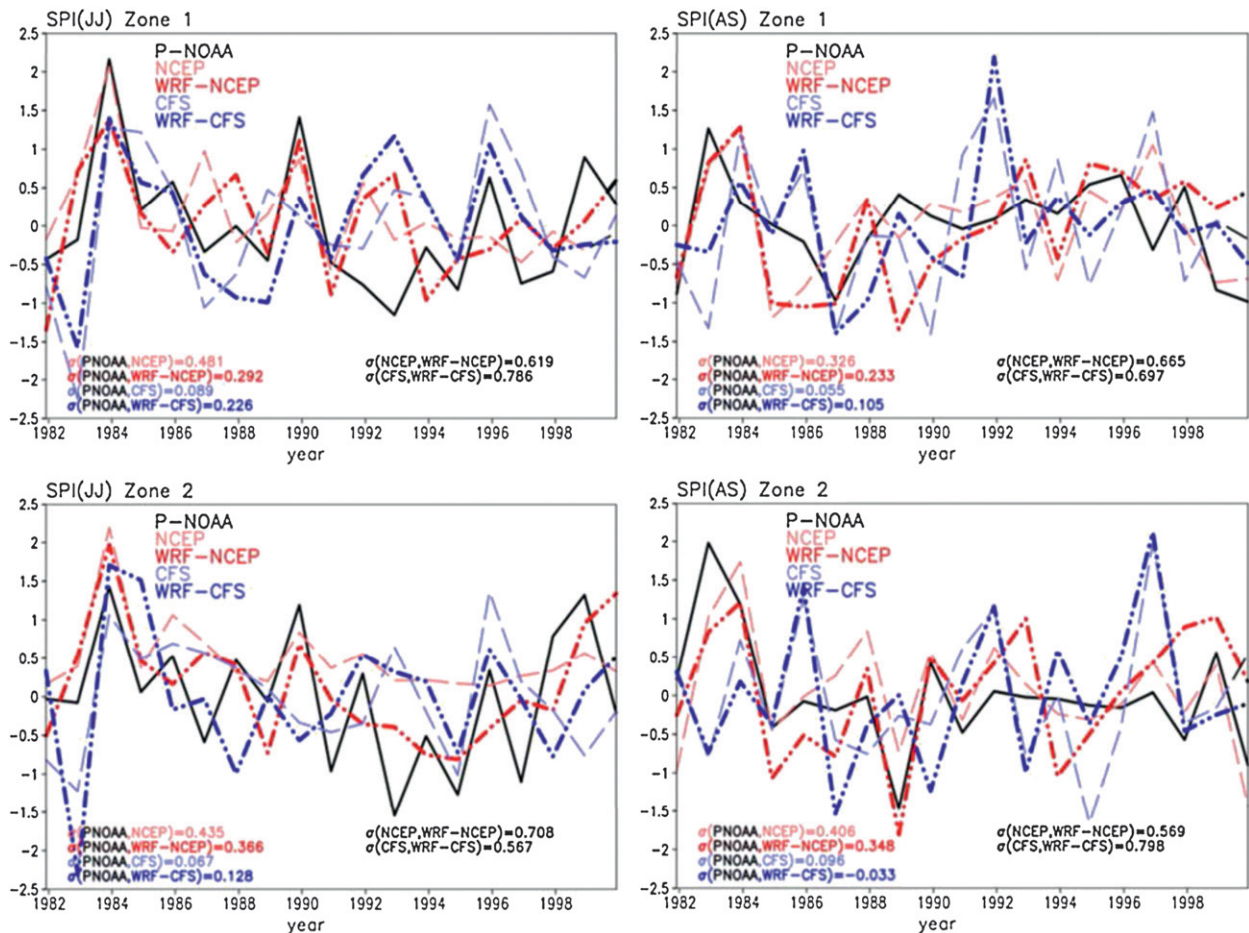


FIG. 13. Early summer (JJ) and late summer (AS) SPI interannual variation from P-NOAA, NCEP–NCAR reanalysis, WRF-NCEP, CFS, and WRF-CFS. The correlations between these data are indicated on the plot.

5. Interannual variability in relation to Pacific SST associated teleconnections

Given the time-varying influence of Pacific SST forcing on summer precipitation, the 500-mb height anomaly correlation between CFS and the NCEP–NCAR reanalysis (Fig. 14) not surprisingly shows a rapid decrease in the ability of CFS to represent the observed large-scale circulation in early versus late part of the warm season in the United States, with the highest anomaly correlation in the United States occurring in the far western United States in JJ, near 0.4. The performance of CFS with respect to representing interannual variability of the large-scale circulation during the warm season is very similar to other GCMs (Liang et al. 2008).

As ENSO PDV is the dominant influence on the continental-scale distribution of NAMS precipitation during the early part of the warm season, how is this represented in CFS and WRF-CFS simulated precipitation in comparison with precipitation observations?

WRF-NCEP is considered equivalent to observations for determination of the dominant modes warm season precipitation variability. Figures 15 and 16 show, respectively, the first two REOF modes of JJ SPI in WRF-NCEP, which explain slightly less than 30% of the total JJ SPI variance, and their relationship with the corresponding 500-mb height anomalies and global SSTA, as the regression on the principal component. The two dominant modes both reveal the expected reverse relationship between early warm season precipitation in the central United States and NAMS region and teleconnection patterns in the 500-mb height anomalies related to monsoon ridge positioning. The first mode is associated more with PDV and the second mode more associated with ENSO, as indicated by the patterns of SSTA, consistent with Castro et al. (2007b). An identical analysis was performed on the equivalent JJ SPI from CFS and WRF-CFS. Figures 17 and 18, respectively, show the statistically significant (at the 95% level), most highly correlated JJ SPI modes from CFS and WRF-CFS and their relationship with CFS

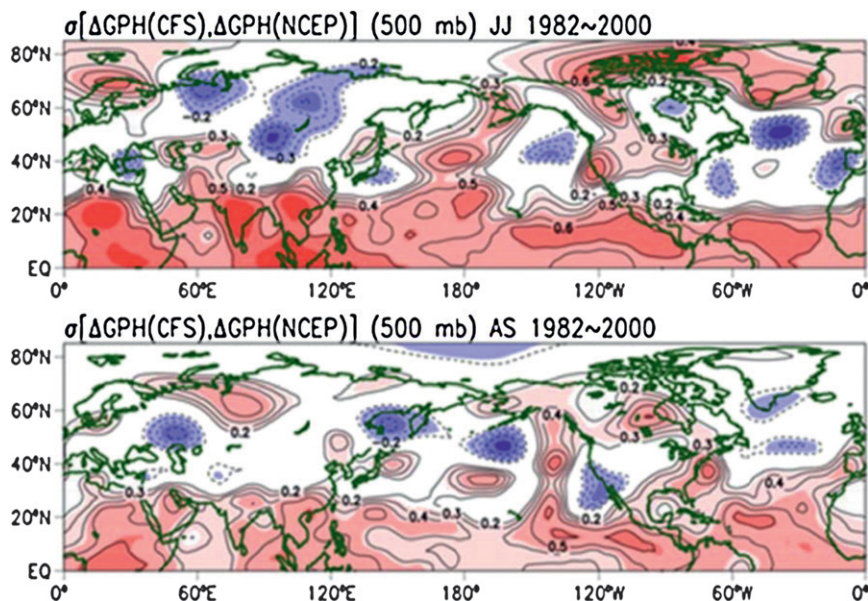


FIG. 14. 500-mb height anomaly correlations between CFS and the NCEP–NCAR reanalysis in (top) early (JJ) and (bottom) late (AS) parts of the summer. Shaded is local significance, and line contour is correlation between CFS and NCEP–NCAR reanalysis.

500-mb height anomalies and global SSTA. Comparing CFS versus WRF-CFS, the RCM substantially improves the ability to represent the influence of ENSO-PDV variability on early warm season precipitation, as WRF-CFS shows a more well-defined reverse relationship between central U.S. and NAMS precipitation and a stronger relationship to 500-mb height anomalies and Pacific SSTA. The teleconnection pattern for WRF-CFS in Fig. 18 reflects more clearly the influence of ENSO on monsoon ridge positioning, and not PDV, and is very similar to Fig. 5 in Castro et al. (2007b). A similar analysis was performed for AS (not shown). We omit showing those results because of the diminished influence of Pacific SST on NAMS and relatively poorer performance of CFS in representing the large-scale atmospheric circulation over the United States at this time (Fig. 14, lower panel). Even though CFS and WRF-CFS both represent the early summer atmospheric circulation and precipitation response to Pacific SST as a statistically distinguishable mode of variability, this does not necessarily mean CFS can always give a good deterministic warm season seasonal forecast. We will illustrate this point in the next section, in specific reference to seasonal forecasts for 1984 and 1993.

6. Concluding points and discussion

Can an RCM improve seasonal forecasts of the North American monsoon? The evidence presented herein

suggests that the answer to this question is a qualified yes, but with several caveats. To represent the NAMS as a salient climatological feature within a dynamical modeling system, a model resolution of at least tens of kilometers is required. We have shown that this is the case for type 2 and type 3 dynamical downscaling. At this resolution, the mesoscale processes that cause thunderstorms are reasonably represented, particularly the diurnal cycle of convection. However, there are spatially coherent differences in the performance of the RCM-simulated precipitation within the NAME tier 2 region, both climatologically and interannually. Even with type 2 dynamical downscaling, an RCM is still quite challenged to represent the propagating, more organized convection that causes monsoon precipitation at a distance from mountainous terrain, westward from the Sierra Madre and Mogollon Rim.

In terms of representing interannual variability of precipitation and temperature anomalies during the warm season, the WRF-CFS simulations tend to slightly increase σ_{anom} in those geographic areas where it is already positive in CFS but does not significantly change its overall spatial pattern. Both CFS and WRF-CFS perform better in forecasting temperature and precipitation in the western United States and NAMS region during the early part of the warm season (JJ), owing to the relatively stronger teleconnectivity between Pacific SSTs and the large-scale atmospheric circulation over North America at this time. Using our objective criteria,

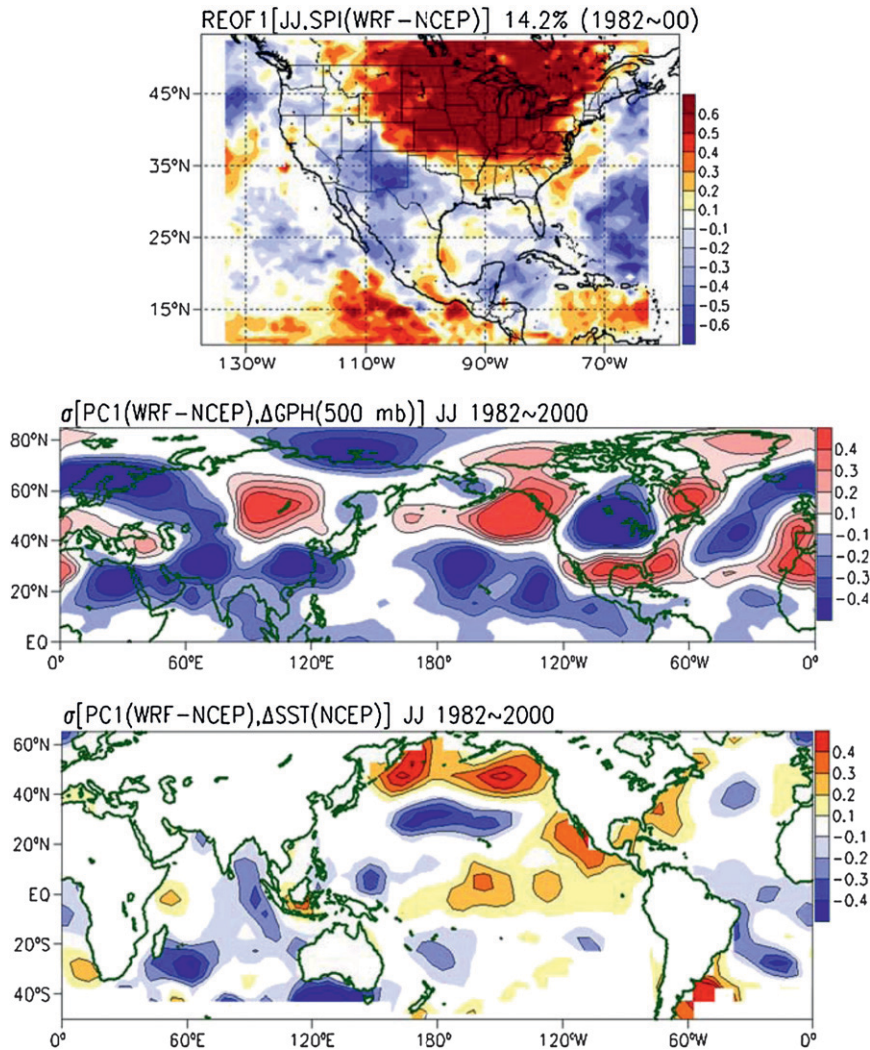


FIG. 15. (top) First REOF of early warm season (JJ) WRF-NCEP SPI, shown as the SPI regression on the principal component (PC) with variance explained. (middle) Corresponding PC correlation on normalized 500-mb geopotential height anomalies from NCEP-NCAR reanalysis. (bottom) Corresponding PC correlation on observed SSTA

WRF-CFS generally adds value to seasonally forecast temperature anomalies in the NAME tier 2 region in JJ for this reason. Although WRF-CFS seasonally forecast precipitation anomalies in the core monsoon region are also slightly higher than CFS in JJ, they are not statistically significant.

In the nine-member ensemble used for this study, CFS represents the early warm season atmospheric teleconnection response associated with ENSO well, but not PDV. That may account for the relatively poor performance of CFS and WRF-CFS in the central United States, where wet or dry conditions in summer are substantially influenced by PDV there (e.g., Schubert et al. 2004). For geographic locations where Pacific SST

variability has a greater influence on monsoon rainfall, as indicated by the dominant spatial loadings of early warm season SPI, an RCM may potentially add some value for seasonal forecasting. Specifically, for the core NAMS region, where WRF-CFS correctly represents a dry (wet) monsoon in association with El Niño-like (La Niña-like) conditions in the Pacific, σ_{anomT} and σ_{anomP} do increase from the driving CFS model. As Pacific SST teleconnectivity to North American climate diminishes in late summer, so too do σ_{anomT} and σ_{anomP} over the entire RCM domain, but especially in the NAMS region.

There is also the question of how the specification of the initial soil moisture in the WRF-CFS simulations

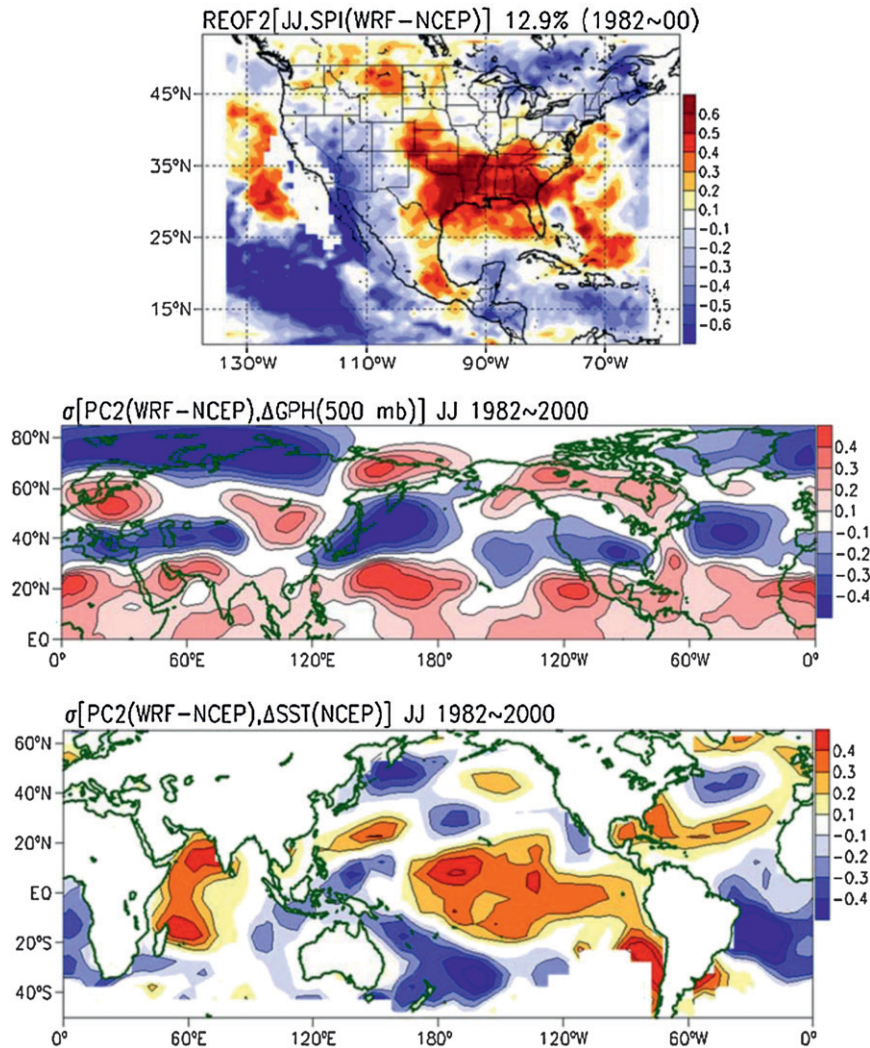


FIG. 16. As in Fig. 15, but for the second REOF of early warm season JJ SPI in WRF-NCEP.

may influence the seasonally forecasted precipitation. Similar to Castro et al. (2007a), we used a predetermined soil moisture analysis (from NARR). To test the sensitivity to this initial soil moisture specification, we conducted an additional WRF-NCEP experiment for the summer of 1993, a year that has been heavily studied in terms of soil moisture feedback processes in the central United States. The additional experiment was initialized with NARR soil moisture at the beginning of May and then compared to the continuous run WRF-NCEP simulation described earlier in section 2. We found that the greatest precipitation differences occurred in the region of the central United States where flooding conditions occurred, consistent with Pan et al. (1996) and Hong and Pan (2000), that suggest the effect of soil moisture feedback is locally confined (results not shown). The continental-scale spatial pattern of warm season

precipitation, tied to Pacific SST forcing, though, was quite similar between the two simulations. Similar sensitivity to the initial soil moisture would thus be expected with the WRF-CFS simulations.

Realizing the full potential to improve NAMS seasonal forecasts with a dynamical downscaling approach depends both on the driving forecast GCM and RCM. Before proceeding with dynamical downscaling of a seasonal forecast GCM, it should first be assessed whether the GCM has a reasonable representation of the warm season atmospheric synoptic-scale circulation, in terms of climatology and interannual variability. For North America, the driving forecast GCM must reasonably represent the atmospheric teleconnection responses associated with ENSO-PDV variability, as this is a principal driver of early warm season precipitation variability. To illustrate the point, Fig. 19 shows the observed and

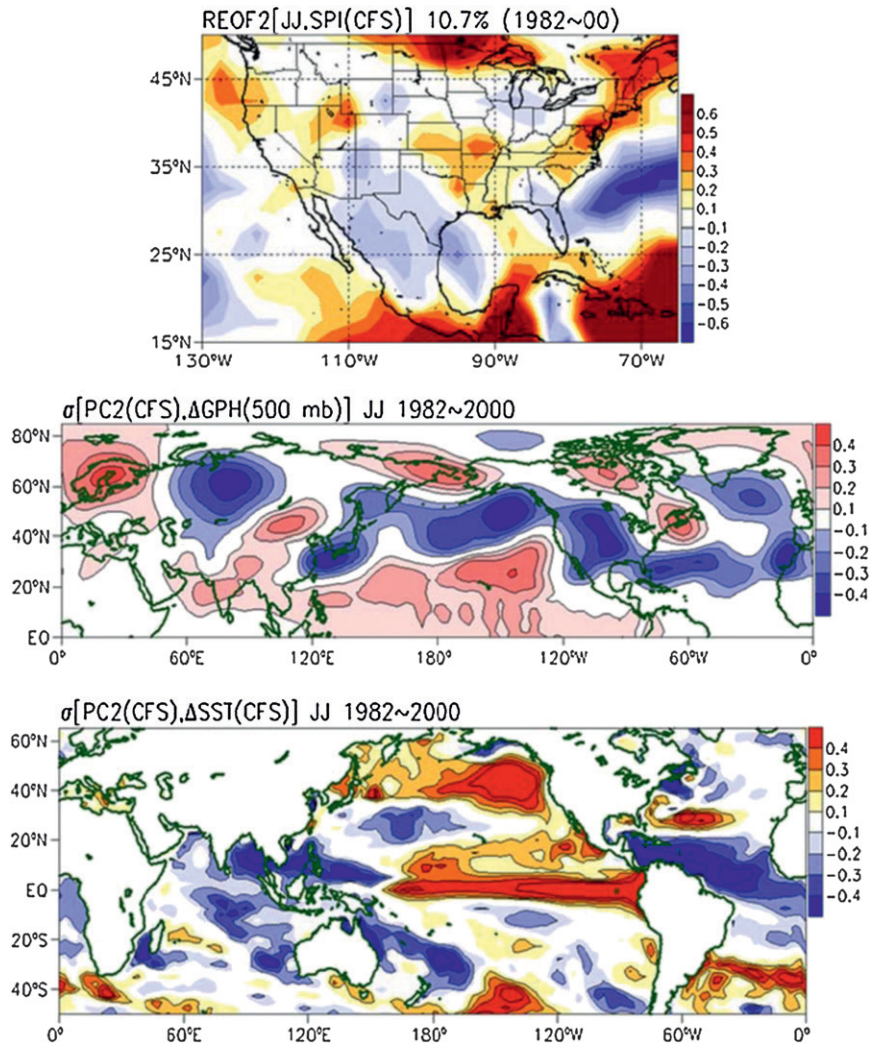


FIG. 17. (top) Most highly correlated mode of early warm season (JJ) SPI in CFS in comparison to the first three REOF early warm season SPI modes from WRF-NCEP, shown as the correlation on the principal component with variance explained. Specifically, this mode is most highly correlated with the second REOF from WRF-NCEP at a value of 0.42 with significance exceeding the 95% level. (middle) Corresponding PC correlation on normalized 500-mb geopotential height anomalies from CFS. (bottom) Corresponding PC correlation on CFS SSTA.

WRF-CFS simulated early warm season SPI for 1984 and 1993 and the corresponding NCEP-NCAR reanalysis and CFS 500-mb heights. These were wettest and driest monsoons, respectively in the 1982–2000 record for NAME precipitation zones 1 and 2. In 1984, CFS reasonably simulates a strong monsoon ridge developing in early summer, leading to a very wet and early monsoon and dry conditions in the central United States. However, in 1993, CFS does not capture the persistent trough over the western United States that helps sustain very wet conditions in the central United States and delay monsoon onset. We have only highlighted

the influence of Pacific SST forcing because it heavily governs CFS predictability in the cool season. Other warm season teleconnections responses during the warm season, such as the circumglobal teleconnection (Ding and Wang 2005) and the influence of the Atlantic (e.g., Sutton and Hodson 2005), are also very important but have not been considered here. Better performing seasonal forecast GCMs should be more heavily weighted in any seasonal forecast scheme that considers multiple seasonal forecast GCMs. This would follow similar strategies that have been used to differentially weight GCMs from the Intergovernmental Panel on Climate

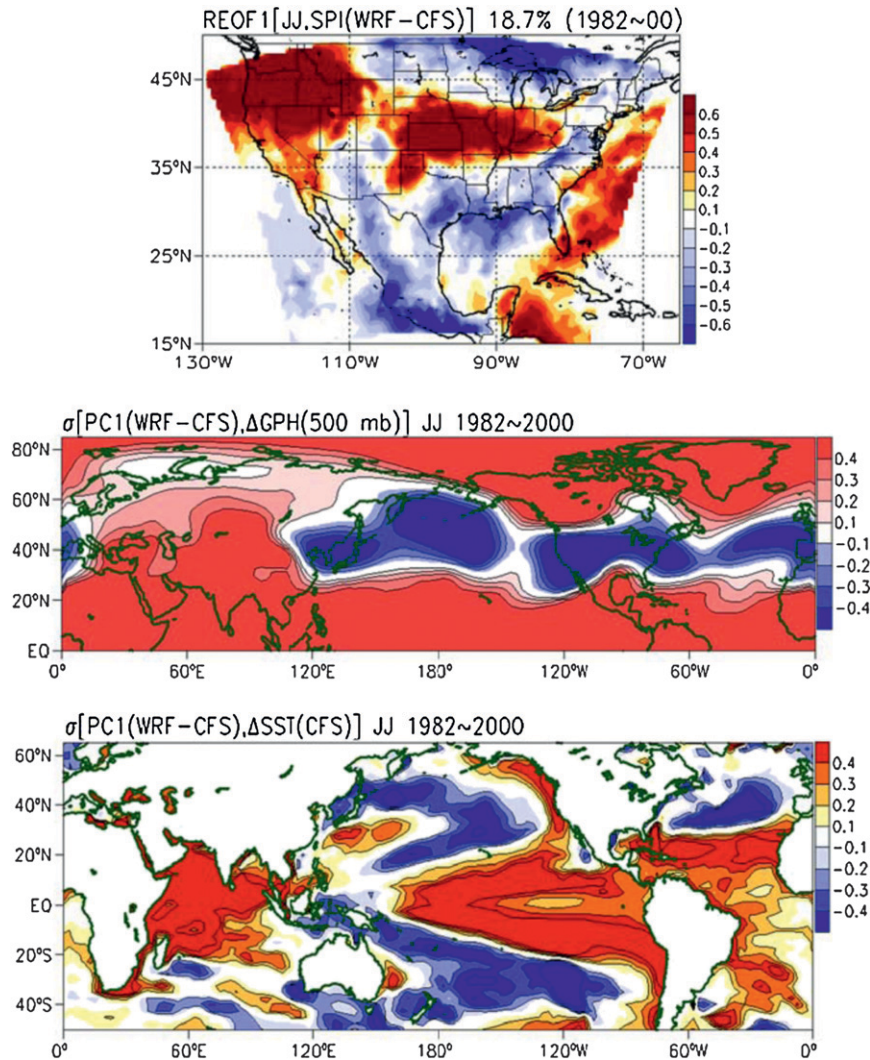


FIG. 18. (top) Most highly correlated mode of early warm season (JJ) SPI in WRF-CFS in comparison to first three REOF early warm season SPI modes from WRF-NCEP, shown as the regression on the principal component with variance explained. Specifically, this mode is most highly correlated with the second REOF from WRF-NCEP at a value of 0.44 with significance exceeding the 95% level. (middle) Corresponding PC correlation on normalized 500-mb geopotential height anomalies from CFS. (bottom) Corresponding PC correlation on CFS SSTA.

Change Fourth Assessment report (IPCC AR4; e.g., Gleckler et al. 2008; Maxino et al. 2008; Dominguez et al. 2010). The maximum possible number of ensemble members should be considered to have the best GCM seasonal forecasts (Saha et al. 2006), and we acknowledge that as a weakness in this study. RCM performance may also improve with increased spatial resolution and/or improvements to convective parameterization schemes. The modified Kain-Fritsch scheme of Truong et al. (2009), with a convective trigger that accounts for the effects of dynamic pressure in complex terrain, can alleviate the

underestimation of precipitation in the WRF-NCEP simulations (Luong et al. 2011). Also, a more sophisticated treatment of the land surface is possible that considers vegetation as a dynamic parameter (Niu et al. 2011; Yang et al. 2011). We hope these suggestions will be helpful in planning the next phase of the Multi-Ensemble Dynamic Downscaling of Multi-GCM Seasonal Forecast (MRED) project (Arritt 2011) to consider North American warm season precipitation, further supporting the incorporation of RCMs a component in NCEP operational seasonal forecasts in the near future.

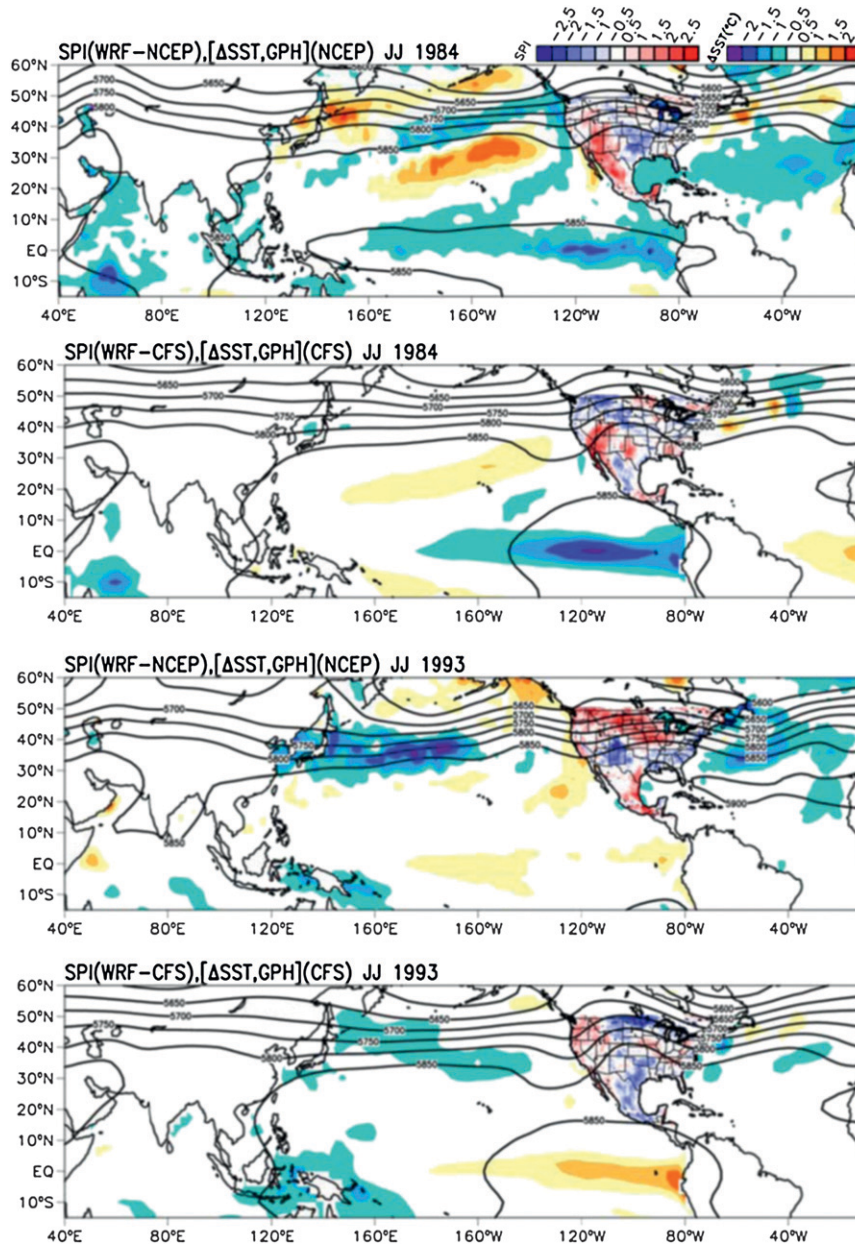


FIG. 19. Early summer (JJ) SPI simulated by WRF-NCEP and WRF-CFS for (top two rows) 1984 and (bottom two rows) 1993 with corresponding NCEP-NCAR reanalysis and CFS global SSTA (shaded) and 500-mb geopotential height (contours). The corresponding SPI and SSTA color bars are shown at top right corner.

Acknowledgments. This work was supported by the National Science Foundation, Grant ATM-813656. We sincerely thank Mr. Matthew Switanek for his assistance in obtaining the CFS model data from NCEP and Drs. Russ Vose and Ed Cook for providing access and guidance in the use of the P-NOAA data. Other observational datasets used in this study were provided by NOAA/OAR/ESRL PSD, Boulder, Colorado, USA from their website (<http://www.esrl.noaa.gov/psd>).

REFERENCES

- Arritt, R. W., 2011: Ensemble downscaling of seasonal forecasts for hydrological applications. Recorded Presentation, *23rd Conf. on Climate Variability and Change and 25th Conf. on Hydrology*, Seattle, WA, Amer. Meteor. Soc., J9.5. [Available online at <https://ams.confex.com/ams/91Annual/webprogram/Paper184836.html>.]
- Barlow, M., S. Nigam, and E. H. Berbery, 1998: Evolution of the North American Monsoon System. *J. Climate*, **11**, 2238–2257.

- Bieda, S. W., III, C. L. Castro, S. L. Mullen, A. Comrie, and E. Pytlak, 2009: The relationship of transient upper-level troughs to variability of the North American monsoon system. *J. Climate*, **22**, 4213–4227.
- Carbone, R. E., J. D. Tuttle, D. A. Ahijevych, and S. B. Trier, 2002: Inferences of predictability associated with warm season precipitation episodes. *J. Atmos. Sci.*, **59**, 2033–2056.
- Castro, C. L., T. B. McKee, and R. A. Pielke Sr., 2001: The relationship of the North American monsoon to tropical and North Pacific sea surface temperatures as revealed by observational analyses. *J. Climate*, **14**, 4449–4473.
- , R. A. Pielke Sr., and G. Leoncini, 2005: Dynamical downscaling: Assessment of value retained and added using the Regional Atmospheric Modeling System (RAMS). *J. Geophys. Res.*, **110**, D05108, doi:10.1029/2004JD004721.
- , —, and J. O. Adegoke, 2007a: Investigation of the summer climate of the contiguous United States and Mexico using the Regional Atmospheric Modeling System (RAMS). Part I: Model climatology (1950–2002). *J. Climate*, **20**, 3844–3865.
- , —, —, S. D. Schubert, and P. J. Pegion, 2007b: Investigation of the summer climate of the contiguous United States and Mexico Using the Regional Atmospheric Modeling System (RAMS). Part II: Model climate variability. *J. Climate*, **20**, 3866–3887.
- , A. B. Beltrán-Przekurat, and R. A. Pielke Sr., 2009: Spatio-temporal variability of precipitation, modeled soil moisture, and vegetation greenness in North America within the recent observational record. *J. Hydrometeorol.*, **10**, 1355–1378.
- Cayan, D. R., M. D. Dettinger, H. F. Diaz, and N. E. Graham, 1998: Decadal variability of precipitation over western North America. *J. Climate*, **11**, 3148–3166.
- Cerezo-Mota, R., M. Allen, and R. Jones, 2011: Mechanisms controlling precipitation in the northern portion of the North American monsoon. *J. Climate*, **24**, 2771–2783.
- Chan, S. C., and V. Mishra, 2011: Dynamic downscaling of the North American monsoon with the NCEP–Scripps regional spectral model from the NCEP CFS global model. *J. Climate*, **24**, 653–673.
- Chou, M.-D., and M. J. Suarez, 1994: An efficient thermal infrared radiation parameterization for use in general circulation models. NASA Tech. Memo. 104606, 85 pp.
- Collier, J. C., and G. J. Zhang, 2007: Effects of increased horizontal resolution on simulation of the North American monsoon in the NCAR CAM3: An evaluation based on surface, satellite, and reanalysis data. *J. Climate*, **20**, 1843–1861.
- Comrie, A. C., and E. C. Glenn, 1998: Principal components-based regionalization of precipitation regimes across the southwest United States and northern Mexico, with an application to monsoon precipitation variability. *Climate Res.*, **10**, 201–215.
- Corbosiero, K. L., M. J. Dickinson, and L. F. Bosart, 2009: The contribution of eastern North Pacific cyclones to the rainfall climatology of the southwest United States. *Mon. Wea. Rev.*, **137**, 2415–2435.
- Daly, C., R. P. Neilson, and D. L. Phillips, 1994: A statistical-topographic model for mapping climatological precipitation over mountainous terrain. *J. Appl. Meteor.*, **33**, 140–158.
- Davies, H. C., 1976: A lateral boundary formulation for multi-level prediction models. *Quart. J. Roy. Meteor. Soc.*, **102**, 405–418.
- Ding, Q., and B. Wang, 2005: Circumglobal teleconnection in the Northern Hemisphere summer. *J. Climate*, **18**, 3483–3505.
- Dominguez, F., J. Cañon, and J. Valdes, 2010: IPCC-AR4 climate simulations for the southwestern U.S.: The importance of future ENSO projections. *Climatic Change*, **99**, 499–514, doi:10.1007/s10584-009-9672-5.
- Douglas, A. V., and P. J. Englehart, 2007: A climatological perspective of transient synoptic features during NAME 2004. *J. Climate*, **20**, 1947–1954.
- Ek, M. B., K. E. Mitchell, Y. Lin, E. Rogers, P. Grunmann, V. Koren, G. Gayno, and J. D. Tarpley, 2003: Implementation of Noah land surface model advancements in the National Centers for Environmental Prediction operational mesoscale Eta model. *J. Geophys. Res.*, **108**, 8851, doi:10.1029/2002JD003296.
- Gao, X., J. Li, and S. Sorooshian, 2007: Modeling intraseasonal features of 2004 North American monsoon precipitation. *J. Climate*, **20**, 1882–1896.
- Gleckler, P. J., K. E. Taylor, and C. Doutriaux, 2008: Performance metrics for climate models. *J. Geophys. Res.*, **113**, D06104, doi:10.1029/2007JD008972.
- Grantz, K., B. Rajagopalan, M. Clark, and E. Zagona, 2007: Seasonal shifts in the North American monsoon. *J. Climate*, **20**, 1923–1935.
- Gutzler, D. S., and Coauthors, 2005: The North American Monsoon Model Assessment Project: Integrating numerical modeling into a field-based process study. *Bull. Amer. Meteor. Soc.*, **86**, 1423–1429.
- Held, I. M., S. W. Lyons, and S. Nigam, 1989: Transients and the extratropical response to El Niño. *J. Atmos. Sci.*, **46**, 163–174.
- Higgins, R. W., Y. Yao, and X. L. Wang, 1997: Influence of the North American monsoon system on the U.S. summer precipitation regime. *J. Climate*, **10**, 2600–2622.
- Higgins, W., and D. Gochis, 2007: Synthesis of results from the North American Monsoon Experiment (NAME) process study. *J. Climate*, **20**, 1601–1607.
- , and Coauthors, 2006: The NAME 2004 field campaign and modeling strategy. *Bull. Amer. Meteor. Soc.*, **87**, 79–94.
- Hong, S.-Y., and H. L. Pan, 2000: Impact of soil moisture anomalies on seasonal summertime circulation over North America in a regional climate model. *J. Geophys. Res.*, **105** (D24), 29 625–29 634.
- , H.-M. H. Juang, and Q. Zhao, 1998: Implementation of prognostic cloud scheme for a regional spectral model. *Mon. Wea. Rev.*, **126**, 2621–2639.
- , J. Dudhia, and S.-H. Chen, 2004: A revised approach to ice-microphysical processes for the bulk parameterization of cloud and precipitation. *Mon. Wea. Rev.*, **132**, 103–120.
- Hutchinson, M. F., D. W. McKenney, K. Lawrence, J. H. Pedlar, R. F. Hopkinson, E. Milewska, and P. Papadopol, 2009: Development and testing of Canada-wide interpolated spatial models of daily minimum-maximum temperature and precipitation for 1961–2003. *J. Appl. Meteor. Climatol.*, **48**, 725–741.
- Janjic, Z. I., 1990: The step-mountain coordinate: Physical package. *Mon. Wea. Rev.*, **118**, 1429–1443.
- , 1996: The surface layer in the NCEP Eta model. Preprints, *11th Conf. on Numerical Weather Prediction*, Norfolk, VA, Amer. Meteor. Soc., 354–355.
- , 2002: Nonsingular implementation of the Mellor–Yamada level 2.5 scheme in the NCEP Meso model. NCEP Office Note 437, 61 pp.
- Kain, J. S., 2004: The Kain–Fritsch convective parameterization: An update. *J. Appl. Meteor.*, **43**, 170–181.
- , and J. M. Fritsch, 1993: Convective parameterization for mesoscale models: The Kain–Fritsch scheme. *The Representation of Cumulus Convection in Numerical Models*, Meteor. Monogr., No. 46, Amer. Meteor. Soc., 165–170.

- Kalnay, E., and Coauthors, 1996: The NCEP/NCAR 40-Year Reanalysis Project. *Bull. Amer. Meteor. Soc.*, **77**, 437–471.
- Kanamitsu, M., and H. Kanamaru, 2007: Fifty-seven-year California reanalysis downscaling at 10 km (CaRD10). Part I: System detail and validation with observations. *J. Climate*, **20**, 5553–5571.
- Kiladis, G. N., and H. F. Diaz, 1989: Global climatic anomalies associated with extremes in the Southern Oscillation. *J. Climate*, **2**, 1069–1090.
- Lang, T. J., D. A. Ahijevych, S. W. Nesbitt, R. E. Carbone, S. A. Rutledge, and R. Cifelli, 2007: Radar-observed characteristics of precipitating systems during NAME 2004. *J. Climate*, **20**, 1713–1733.
- Lau, N.-C., 1985: Modeling the seasonal dependence of the atmospheric response to observed El Niños in 1962–76. *Mon. Wea. Rev.*, **113**, 1970–1996.
- Lee, M.-I., and Coauthors, 2007: Sensitivity to horizontal resolution in the AGCM simulations of warm season diurnal cycle of precipitation over the United States and northern Mexico. *J. Climate*, **20**, 1862–1881.
- Legates, D. R., and C. J. Willmott, 1990: Mean seasonal and spatial variability global surface air temperature. *Theor. Appl. Climatol.*, **41**, 11–21.
- Liang, X.-L., J. Zhu, K. E. Kunkel, M. Ting, and J. X. L. Wang, 2008: Do CGCMs simulate the North American monsoon precipitation seasonal interannual variability? *J. Climate*, **21**, 4424–4448.
- Lin, Y.-L., R. D. Rarley, and H. D. Orville, 1983: Bulk parameterization of the snow field in a cloud model. *J. Appl. Meteor.*, **22**, 1065–1092.
- Liston, G. E., and R. A. Pielke Sr., 2000: A climate version of the Regional Atmospheric Modeling System. *Theor. Appl. Climatol.*, **66**, 29–47.
- Livezey, R. E., and M. M. Timonfeyeva, 2008: The first decade of long-lead U.S. seasonal forecasts. *Bull. Amer. Meteor. Soc.*, **89**, 843–854.
- Luong, T., C. L. Castro, and W. Cassell, 2011: Improvement in the representation of warm season convective precipitation in complex terrain using a modified Kain–Fritsch convective parameterization scheme. *Proc. Sixth Southwest Hydrometeorology Symp.*, Tempe, AZ, NOAA. [Abstract available online at <http://www.wrh.noaa.gov/psr/pns/symposium/abstracts.pdf>]
- Maddox, R. A., D. M. McCollum, and K. W. Howard, 1995: Large-scale patterns associated with severe summertime thunderstorms over central Arizona. *Wea. Forecasting*, **10**, 763–778.
- Maxino, C. C., B. J. McAvaney, A. J. Pitman, and S. E. Perkins, 2008: Ranking the AR4 climate models over the Murray–Darling basin using simulated maximum temperature, minimum temperature and precipitation. *Int. J. Climatol.*, **28**, 1097–1112.
- McCabe, G. J., and M. D. Dettinger, 1999: Decadal variations in the strength of ENSO teleconnections with precipitation in the western United States. *Int. J. Climatol.*, **19**, 1399–1410.
- McKee, T. B., N. J. Doesken, and J. Kleist, 1993: The relationship of drought frequency and duration to time scales. Preprints, *Eighth Conf. on Applied Climatology*, Anaheim, CA, Amer. Meteor. Soc., 179–184.
- Mesinger, F., and Coauthors, 2006: North American Regional Reanalysis. *Bull. Amer. Meteor. Soc.*, **87**, 343–360.
- Miguez-Macho, G., G. L. Stenchikov, and A. Robock, 2005: Regional climate simulations over North America: Interaction of local processes with improved large-scale flow. *J. Climate*, **18**, 1227–1246.
- Mlawer, E. J., S. J. Taubman, P. D. Brown, M. J. Iacono, and S. A. Clough, 1997: Radiative transfer for inhomogeneous atmospheres: RRTM, a validated correlated-*k* model for the longwave. *J. Geophys. Res.*, **102** (D14), 16 663–16 682.
- Nesbitt, S. W., D. J. Gochis, and T. J. Lang, 2008: The diurnal cycle of clouds and precipitation along the Sierra Madre Occidental observed during NAME-2004: Implications for warm season precipitation estimation in complex terrain. *J. Hydrometeorol.*, **9**, 728–743.
- Niu, G.-Y., and Coauthors, 2011: The community Noah land surface model with multi-parameterization options (Noah-MP): 1. Model description and evaluation with local-scale measurements. *J. Geophys. Res.*, **116**, D12109, doi:10.1029/2010JD015139.
- Pan, Z., E. Takle, M. Segal, and R. Turner, 1996: Influences of model parameterization schemes on the response of rainfall to soil moisture in the central United States. *Mon. Wea. Rev.*, **124**, 1786–1802.
- Piechota, T. C., and J. A. Dracup, 1996: Drought and regional hydrologic variations in the United States: Associations with the El Niño–Southern Oscillation. *Water Resour. Res.*, **32**, 1359–1373.
- , —, and R. G. Fovell, 1997: Western U.S. streamflow and atmospheric circulation patterns during El Niño–Southern Oscillation. *J. Hydrol.*, **201**, 249–271.
- Ray, A. J., G. M. Garfin, M. Wilder, M. Vásquez-León, M. Lenart, and A. C. Comrie, 2006: Applications of monsoon research: Opportunities to inform decision making and reduce regional vulnerability. *J. Climate*, **20**, 1608–1627.
- Redmond, K. T., and R. W. Koch, 1991: Surface climate and streamflow variability in the western United States and their relationship to large-scale circulation indices. *Water Resour. Res.*, **27**, 2381–2399.
- Richman, M. B., 1986: Rotation of principal components. *J. Climatol.*, **6**, 293–335.
- Rockel, B., C. L. Castro, R. A. Pielke Sr., H. von Storch, and G. Leoncini, 2008: Dynamical downscaling: Assessment of model system dependent retained and added variability for two different regional climate models. *J. Geophys. Res.*, **113**, D21107, doi:10.1029/2007JD009461.
- Ropelewski, C. F., and M. S. Halpert, 1986: North American precipitation and temperature patterns associated with the El Niño–Southern Oscillation (ENSO). *Mon. Wea. Rev.*, **114**, 2352–2362.
- Saha, S., and Coauthors, 2006: The NCEP Climate Forecast System. *J. Climate*, **19**, 3483–3517.
- Schemm, J.-K., R. W. Higgins, L. Long, and W. Shi, 2009: The North American monsoon forecast forum at CPC and assessment of the NCEP CFS GCM. *Proc. Fifth Symp. on Southwest Hydrometeorology*, Albuquerque, NM, NOAA/NWS. [Available online at http://www.srh.noaa.gov/media/abq/sswhm/schemm_etal_sw_hydromet_09.pdf]
- Schneider, J. M., and J. D. Garbrecht, 2005: Recent utility of NOAA/CPC seasonal precipitation climate forecasts. *Climate Variations, Climate Change, and Water Resources Engineering*, J. D. Garbrecht and T. C. Piechota, Eds., American Society of Civil Engineers, 51–64.
- Schubert, S. D., M. J. Suarez, P. J. Pegion, R. D. Koster, and J. T. Bacmeister, 2004: Causes of long-term drought in the U.S. Great Plains. *J. Climate*, **17**, 485–503.
- Shepard, D., 1968: A two-dimensional interpolation function for irregularly-spaced data. *Proceedings of the 1968 ACM National Conference*, Association for Computing Machinery, 517–524.
- Skamarock, W. C., J. B. Klemp, J. Dudhia, D. O. Gill, D. M. Barker, W. Wang, and J. G. Powers, 2005: A description of the

- Advanced Research WRF version 2. NCAR Tech. Note NCAR/TN-468+STR, 88 pp.
- Sutton, R. T., and D. L. R. Hodson, 2005: Atlantic Ocean forcing of North American and European summer climate. *Science*, **309**, 115–118, doi:10.1126/science.1109496.
- Tribbia, J. J., 1991: The rudimentary theory of atmospheric teleconnections associated with ENSO. *Teleconnections Linking Worldwide Climate Anomalies*, M. H. Glantz, R. W. Katz, and N. Nicholls, Eds., Cambridge University Press, 285–308.
- Truong, N. M., T. T. Tien, R. A. Pielke Sr., C. L. Castro, and G. Leoncini, 2009: A modified Kain–Fritsch scheme and its application for simulation of an extreme precipitation event in Vietnam. *Mon. Wea. Rev.*, **137**, 766–789.
- von Storch, H., H. Langenberg, and F. Feser, 2000: A spectral nudging technique for dynamical downscaling purposes. *Mon. Wea. Rev.*, **128**, 3664–3673.
- Wilks, D., 2006: *Statistical Methods in the Atmospheric Sciences*. 2nd ed. Academic Press, 627 pp.
- Willmott, C. J., and K. Matsuura, 1995: Smart interpolation of annually averaged air temperature in the United States. *J. Appl. Meteor.*, **34**, 2577–2586.
- , C. M. Rowe, and W. D. Philpot, 1985: Small-scale climate maps: A sensitivity analysis of some common assumptions associated with grid-point interpolation and contouring. *Amer. Cartogr.*, **12**, 5–16.
- Yang, S., Y. Jiang, D. Zheng, R. W. Higgins, Q. Zhang, V. E. Kousky, and M. Wen, 2009: Variations of U.S. regional precipitation and simulations by the NCEP CFS: Focus on the southwest. *J. Climate*, **22**, 3211–3231.
- Yang, Z.-L., and Coauthors, 2011: The community Noah land surface model with multiparameterization options (Noah-MP): 2. Evaluation over global river basins. *J. Geophys. Res.*, **116**, D12110, doi:10.1029/2010JD015140.